UNIVERSITAT POLITÈCNICA DE CATALUNYA
BARCELONATECH

**Escola Tècnica Superior d'Enginyeria
de Telecomunicació de Barcelona**

SMOS-based algorithm to predict potential fire propagation in Europe

A Master's Thesis
Submitted to the Faculty of the
Escola Tècnica d'Enginyeria de Telecomunicació de Barcelona
Universitat Politècnica de Catalunya

Afonso Caldeira Espinha Pinheiro Castela

In partial fulfilment
of the requirements for the degree of
MASTER IN TELECOMMUNICATIONS ENGINEERING

Advisors: Dr. David Chaparro, Dr. Mercè Vall-llossera and Dr.
António Rodrigues

Barcelona, 25th July 2019

Abstract

Climate change raises global temperatures, as well as the duration of droughts in some regions of the globe. These shifts may increase the propagation and frequency of wildfires. In this context, Earth Observation (EO) satellites permit to track conditions related to fire risk on a regular basis and with global coverage. In this study, the focus is put on the water content of soils, a crucial factor on forest fires propagation. Here, soil moisture data from the Soil Moisture and Ocean Salinity (SMOS) mission – as well as information on surface temperature, land cover, ecoregions and the time of fires burning- are applied to estimate the potential risk of fire propagation in Europe. The main objectives are: (i) to study the relationship between soil moisture (SM), land surface temperature (LST) and the wildfires in the European Union (EU) for the period 2010-2018, and (ii) to develop a model to predict the maximum fire spread of wildfires in the EU.

Different models are proposed and tested. Firstly, regressions between (i) burned area and soil moisture and (ii) burned area and surface temperature, are computed. Secondly, SM and LST are combined in a bilinear model, following previous research with similar variables conducted in the Iberian Peninsula. Thirdly, a more complex model is built including interactions of moisture and temperature with land cover, European ecoregions and the month of the fire outbreak.

Results show that SM and LST limit fire spread, and that SMOS-derived data explains between 25% and 73% of fire propagation variance (depending on the model chosen). Comparison among models, as well as their validation, reports that the SM-burned area regression leads to the best fitting ($R^2 = 0.73$) and the lowest error (215 ha) once an additive term (i.e., σ of the logarithm of burned area) is applied to the algorithm.

In conclusion, the model combining burned area and moisture achieves good results and is valid for estimating the risk of propagation of wildfires in Europe. In addition, an example of fire propagation risk map is shown and will be put in operational applications. This study confirms the capacity of L-band soil moisture data to contribute to fire risk assessment, and expands previous applications of microwave-derived moisture information to Europe.

Contents

List of tables

List of figures

1. Introduction

1.1. Motivation and main goal

Human activity increases greenhouse gas (GHGs) emissions, consequently raising global temperatures and the duration of droughts in some regions (Oppenheimer et al. 2015). In particular, global temperatures have increased by ~0.2°C per decade over the last decades, possibly leading to changes in the global water cycle which include more severe and widespread droughts in some regions (Jolly et al., 2015). This leads to more dangerous conditions in terms of the risk of ignition and propagation of wildfires and, in turn, these changes on fire patterns could increment gas emissions reinforcing global warming (e.g., the CO_2 emitted from these events can exceed 50% of fossil fuel combustion emissions; Jolly et al., 2015).

Moreover, human factors such as roads and population density play an important role in fire ignition. For instance, in the Mediterranean region it is estimated that 95% of wildfires are human-caused. This high percentage is also observed in other regions, for example in southern Asia (90%), South America (85%) and northeastern Asia (80%; FAO, 2006). Also, recent data analyses from the European Forest Fires Information System (EFFIS) show that approximately 95% of fires in Europe are human-induced (San-Miguel-Ayanz et al., 2012). Although in some areas natural fires are necessary to maintain the ecosystem's dynamics, most wildfires burning directly or indirectly due to human actions cause huge damage in environmental and economic terms, affecting millions of hectares of vegetation and threatening human lives (FAO, 2006).

In this context, it is essential to study the prior conditions igniting wildfires and favouring their propagation. It is essential to take into account that dry weather (i.e., high temperatures, low precipitation amount, and dry soil and vegetation conditions), as well as wind speed, influence fire spread (Jolly et al. 2015).

Earth Observation (EO) satellites permit to track such conditions worldwide and on a regular basis. In the case of this research, the focus is put on the water content of soils, as well as on surface temperature, in order to determine drought conditions posing risk of fire propagation. To that purpose, passive microwave EO satellites have proved to be very helpful as their measurements are sensitive to water content in soils. Specifically, the first space mission committed to soil moisture monitoring has L-band microwave sensors on board. This is the Soil Moisture and Ocean Salinity (SMOS, launched by the European Space Agency in November 2009).

This study will focus on the applicability of SMOS data, complementarily to other variables, as the basis to estimate the potential extension of wildfires in Europe.

1.2. Theoretical background and state of the art

1.2.1. Theoretical background: microwave radiometry

Electromagnetic waves from the Sun reach the surface of the Earth and are either absorbed or reflected. When thermal equilibrium is reached the absorbed radiation is emitted. This radiation from earth depends on the surface properties and on the wavelength. Measuring it in the microwaves region of the spectrum provides principally two advantages that are important for this work: (i) emissions on the microwaves' part of the spectrum are very sensitive to soil moisture, and (ii) measuring such emissions can be done regardless of weather conditions (i.e., clouds do not mask these emissions).

Microwave's emissions can be measured with high accuracy by radiometers. These are passive sensors that measure the amount of radiation emitted by a source. Hereafter, the main concepts of microwave radiometry are presented:

A. Black body radiation and the Rayleigh-Jeans law

A black body is a theoretical concept which defines an ideal material that absorbs and radiates all the incident energy. The emission of a black body at microwave wavelengths is directly obtained from the brightness (B_f), which is approximately proportional to the physical temperature of the body (T) at microwave frequencies:

$$B_f \sim \frac{2f^2 k_B T}{c^2} = \frac{2k_B T}{\lambda^2},$$ (1.1)

where f is the frequency of the wave in Hz, $k_B = 1.38 \cdot 10^{-23}$ J/K is the Boltzmann's constant, $c = 3 \cdot 10^8$ m/s is the speed of light, and $\lambda = c/f$ is the wavelength. Eq. (1.1) is known as the Rayleigh-Jeans law and it is an approximation of the Planck's radiation law for low frequencies (see Ulaby et al., 1981, pp. 197-198, for more detail on the relationship between both laws).

According to the Rayleigh-Jeans law, the brightness of a black body (B_{bb}) for a specific temperature (T) and bandwidth (Δf) is expressed as:

$$B_{bb} \sim B_f \cdot \Delta f = \frac{2k_B T}{\lambda^2} \cdot \Delta f,$$ (1.2)

B. Grey body radiation

Black bodies are just a theoretical concept useful to understand the notion of brightness. Real bodies, present in nature, do not absorb and transmit all the energy that reach them. This energy is partially absorbed and the rest is reflected. Therefore, it is defined the brightness temperature of a grey body ($T_{RB}(\theta, \phi)$) as the temperature a blackbody would have to produce the brightness emitted by the studied grey body. The brightness temperature is not a real temperature, but an effective one.

Hence, the brightness of a grey body is defined as follows:

$$B(\theta, \phi) \sim \frac{2k_B T_{RB}(\theta,\phi)}{\lambda^2} * \Delta f, \qquad (1.3)$$

The ratio that relates the brightness of grey and black bodies is called emissivity ($e(\theta, \phi)$):

$$e(\theta, \phi) = \frac{B(\theta,\phi)}{B_{bb}} = \frac{T_{RB}(\theta,\phi)}{T} \qquad (1.4)$$

Emissivity ranges from 0 (a perfect reflector) to 1 (a perfect emitter). Then from Eq. (1.4), it is derived that the brightness temperature emitted by a grey body cannot be higher than that of a black body.

C. Measuring brightness temperatures from space

The apparent temperature of an antenna $T_{AP}(\theta,\phi)$ is used to characterize the total brightness incident to the antenna $B_i(\theta, \phi)$:

$$B_i(\theta, \phi) \sim \frac{2k_B T_{AP}(\theta,\phi)}{\lambda^2} * \Delta f, \qquad (1.5)$$

The apparent temperature is linked to the power received by the antenna (see Ulaby et al., 1981, p. 203) and it is a function of different contributions in the case of an Earth-looking radiometer:

$$T_{AP}(\theta, \phi) = T_{UP} + \frac{1}{L_a}(T_B + T_{SC}), \qquad (1.6)$$

where T_{UP} is the brightness temperature of the atmospheric upwelling radiation, L_a is the attenuation of the atmosphere on the radiation emitted by the Earth's surface, T_B is the brightness temperature of the observed scene, and T_{SC} is the downwelling atmospheric radiation scattered by the Earth's surface. The atmospheric effects are negligible at the L-band (1-2 GHz) microwave frequency, range used in soil moisture remote sensing.

Satellites' radiometers transform the radiation collected by the antenna into brightness temperature information. The performance of this process is determined by (i) the radiometric sensitivity, which determines the minimum value of brightness that the antenna is able to discriminate; (ii) the radiometric accuracy, determining how close the readings are to the real values, and (iii) the spatial resolution, which is the closest distance at which the radiometer can obtain different measures coming from two different points.

Radiometric measurements of the Earth surface (over land) are linked to soil emissions and to the effect of vegetation on such emissions. Soil emissions depend on the dielectric constant (ε): a

property of materials which defines the impedance found by an electromagnetic wave passing through them. The dielectric constant of soils is expressed as a complex number ($\varepsilon_s = \varepsilon'_s + j\varepsilon''_s$), where the real part ($\varepsilon'_s$) determines the propagation of the energy through the material, and the imaginary part ($j\varepsilon''_s$) determines the energy losses. Dry soils have a much lower dielectric constant ($\varepsilon = 4$) than water ($\varepsilon = 80$). This is crucial in soil moisture remote sensing, as the dielectric constant of soil-water mixtures rises with increasing water content: from $\varepsilon = 4$ in dry soils to $\varepsilon \sim 40$ in wet soils. As a result, at microwave frequencies, the emission of the soil is linked to the soil water content by the dielectric constant. The emissivity of dry soils ($e(\theta, \phi) \sim 0.95$) decreases with increasing water until soil saturates ($e(\theta, \phi) \sim 0.60$; Schmugge et al., (1986)). Nevertheless, other factors influence the emissivity of soils and must be considered: soil texture and density, soil roughness, temperature, salinity, and the wavelength. Note that longer wavelengths provide information from deeper soil layers. In that sense, L-band radiometers allow capturing soil moisture conditions approximately from the top 5 cm of soils (although in dry soils this can be deeper).

Besides considering soil properties and their role on soil emissions, it is also important to understand the effect of vegetation on these emissions (i.e., mainly, attenuation and scattering). A simple and very used model that takes the effect of vegetation into account is the τ-ω model:

$$T_{Bp} = e_p T_s \gamma \; + \; (1 - \omega) T_\vartheta (1 - \gamma) \; + \; (1 - e_p)(1 - \omega) T_\vartheta (1 - \gamma)\gamma, \qquad (1.8)$$

where p stands for polarization (horizontal or vertical) T_{Bp} is the brightness temperature, e_p is the soil emissivity, T_s and T_ϑ refer to the effective temperatures of soil and vegetation, respectively, ω is the single scattering albedo, and γ is the vegetation transmissivity. Eq. (1.8) is divided in 3 terms: the first one represents the radiation of the soil when attenuated by the vegetation; the second defines the upwards radiation directly emitted by the vegetation; and the third expresses the downwards radiation from the vegetation, after being reflected by the soil and attenuated by the canopy layer.

SMOS has a sun-synchronous polar orbit passing over the equator at 6 a.m. and 6 p.m. when temperature differences between soil and vegetation are minimum. Then, Eq. (1.8) using the approximation $T_\vartheta = T_s$:

$$T_{Bp} = [e_p \gamma \; + \; (1 - \omega)(1 - \gamma) \; + \; (1 - e_p)(1 - \omega)(1 - \gamma)\gamma] T_s \; , \qquad (1.9)$$

1.2.2. L-band satellites and products

At present, there are various microwave-based soil moisture products available. These are mainly obtained from (i) the SMOS and SMAP missions (L-band radiometers); (ii) the Advanced SCATterometer (ASCAT; C-band); and (iii) the Advanced Microwave Scanning Radiometer 2 (AMSR2; C-and X-bands).

The interest of the scientific community for L-band (1.4 GHz) microwave remote sensing has increased during last decades. One of the main reasons is that at low microwave frequencies the emissivity of land and oceans are strong functions of soil moisture and salinity, respectively. As a result, satellite observations of brightness temperature of Earth's surface are used to produce global maps of soil moisture (Kerr et al., 2010). In that sense, the European Space Agency (ESA) launched in November 2009, the SMOS satellite with the objective of retrieving soil moisture (SM) and sea surface salinity (SSS) at a global scale (see Figure 1).
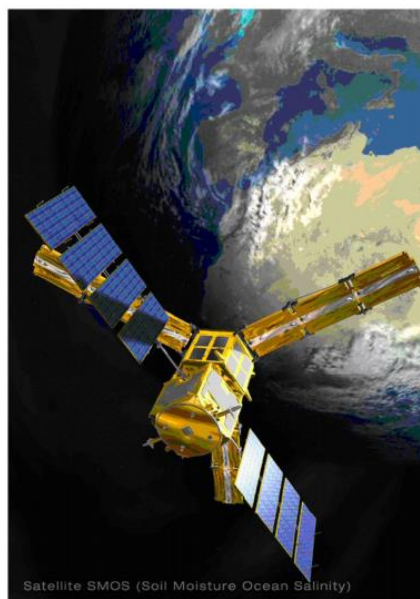
Figure 1. Artists view of SMOS. Source: Kerr, Y et al. (2010)

SMOS orbits the Earth at an altitude of 758 km, following a sun-synchronous orbit, and has a revisit time of 3 days. Its spatial resolution is of ~40 km. The BEC (Barcelona Expert Center) is a joint initiative of the Institut de Ciències del Mar (ICM) and Universitat Politècnica de Catalunya (UPC) for producing and distributing SMOS data at several processing levels. Level 0 (L0) contains the raw data. Level 1 (L1) is divided in three steps. Firstly, L1A products are snapshots going from one pole to the other. Secondly, L1B is the reconstruction of the images of the observations. Lastly, L1C corresponds to a level 1B product reorganized with the angular brightness temperatures at the top of the atmosphere. Level 2 (L2) data provides global surface moisture maps for approximately the soil top 5 cm, with a target accuracy of 0.04 $m^3 \cdot m^{-3}$, and a spatial resolution of ~40 km (Kerr et al., 2010). Level 3 (L3) products combine the images from L2 into a global map of SM and are provided in a regular 25 km grid (the Equal-Area Scalable Earth Grid 2; EASE2) and in standard format (e.g., GRIB files; BEC, 2018). Spatial resolutions at L2 and L3 are too coarse for local and regional applications such as wildfire risk assessment. To bridge this gap, the Barcelona Expert Centre (BEC) facilities provide an enhanced SM

10

product (this is, a L4 product), which is downscaled from the original resolution to 1 km scale using the downscaling method described in Piles et al., (2014) and Portal et al. 2018.

After SMOS, the second L-band mission containing a microwave radiometer was launched in January 2015 by the National Aeronautics and Space Administration (NASA). This satellite is called Soil Moisture Active-Passive (SMAP). Its orbit is sun-synchronous, at an altitude of 685 km, and it has a revisit time of between 2 and 3 days. Its resolution is approximately 40km. Soil emission measurements are obtained at a constant incidence angle of 40º (Entekhabi et al., 2010). Also, note that the Aquarius satellite also operated an L-band radiometer (Le Vine et al., 2010). It was launched on June 2010 and ceased its operations on June 2015.

1.2.3. State of the art

Most fire risk indices are based in meteorological factors. For instance, the well-known Fire Weather Index (FWI, Van Wagner, 1987) uses meteorological data (temperature, rain, wind, and relative humidity), in order to build its six components, which ultimately determine the fire risk level. Among its components, FWI contains information on soil moisture considering the surface, the medium depth and the deep organic matter. Similarly, the McArthur Forest Fire Danger Index (FFDI; McArthur, 1967) is based on moisture of dead fuels, which is tightly linked to the surface soil moisture.

This illustrates the importance of water content in soils to predict the risk of fire spread and suggests that fire risk models could be improved by using EO data. In particular, L-band missions could contribute to this progress because the surface humidity is obtained at a global scale on a time-regular basis, reducing the dependence of fire risk models on meteorological stations (which are usually irregularly distributed and do require interpolation methods to extrapolate their information).

Previous research has focused on satellite-derived soil moisture data to understand the relationship between moisture and fires. For example, Aubrecht et al. (2011) studied the soil water index (SWI) from the sensor Advanced SCATterometer (ASCAT) and found strong spatial correlation between dry soils and detected fires. Forkel et al. (2012) studied the relationship between fires and soil moisture in Lake Baikal, Siberia. In this case, the authors used the surface moisture product derived from the Advanced Microwave Scanning Radiometer - Earth Observing System (AMSR-E) for fires that occurred in 2003, mostly in permafrost soils, which presented negative surface moisture anomalies. They concluded that in the previous year (2002) the lack of precipitation during summer led to soils storing scarce amount of water when freezing on winter. And as a consequence, during the 2003 spring the ice melting released low water to soils, leading to the negative moisture anomalies detected by the satellite. This situation led to unfavourable conditions that preceded the large amount of fires that occurred during 2003's summer.

Later, the relationship between soil moisture, surface temperatures, and fire propagation, has been widely studied for the Iberian Peninsula. In that sense, firstly, Chaparro et al. (2016a) demonstrated that the combined use of surface moisture (SM) and land surface temperature (LST) could lead to obtain reliable fire risk indices based on L-band SMOS products. The authors developed a model to estimate the potential propagation of wildfires based on SM-LST data and auxiliary information. This model reached 83.3% of accuracy with a maximum error of 40.5 ha. Secondly, Chaparro et al. (2016b) focused

on wildfires that burn under temperature and moisture anomalous conditions. The authors concluded that the largest fires took place in the Mediterranean regions under dry and hot soils, and that anomalous dry and warm soil conditions resulted in large number of fires burning out of summer season in the northern Iberian Peninsula.

These studies demonstrated that the role of satellite-derived soil moisture in fire risk assessment is very promising, and that its operational applicability is feasible. Actually, emerging from Chaparro et al. (2016a), the BEC will routinely provide models of potential burned area for the Iberian Peninsula through its website (at the moment of writing, models are being implemented).

The present work aims to extent this model to the European Union, taking profit of the newly released 1 km soil moisture maps, which are provided as an L4 product for Europe at BEC (BEC, 2018). The resulting product could be of great applicability for assessing the risk of potential fire propagation through the continent.

1.3. Objectives

The main objectives of this research are: (i) to study the relationship among soil moisture, land surface temperature and the propagation of wildfires in Europe for the period June 2010 – December 2018, and (ii) to develop a model –mainly based on SMOS soil moisture- predicting the the maximum potential burned area in the European Union.

1.4. Thesis Outline

This work is organized in the following chapters:

- o **Chapter 1** explains the motivation of the study, the applicability of passive microwaves remote sensing on fire risk assessment, and the objective of this thesis.
- o **Chapter 2** describes the study area, the creation of database, and the statistical procedures used to define the fire propagation model.
- o **Chapter 3** presents the results of the fire risk model, as well as its validation.
- o **Chapter 4** discusses the results and puts emphasis on their applicability.
- o **Chapter 5** provides main conclusions of this work and gives suggestions for future work.

2. Material and Methods

2.1. Data

This study focuses on the wildfires burned in the European Union (EU) from June 2010 to December 2018. Fires information is obtained from the European Forest Fires Information System (EFFIS; San-Miguel-Ayanz et al., 2012) database, which registers fires larger than 10 ha occurring in the EU. This dataset includes the date of fire ignition, the burned area, and the location of the wildfire, as well as its georeferenced perimeter.

The EFFIS database registered 7,569 fires larger than 10 ha in the study area between June 2010 and December 2018 (Figure 2). These fires were irregularly distributed among years, being 2017 the year with more fire episodes and 2014 the one with less burnings (Table 1). Most fires burned less than 1,000 ha, although near 500 fires affected larger extensions (Table 2).
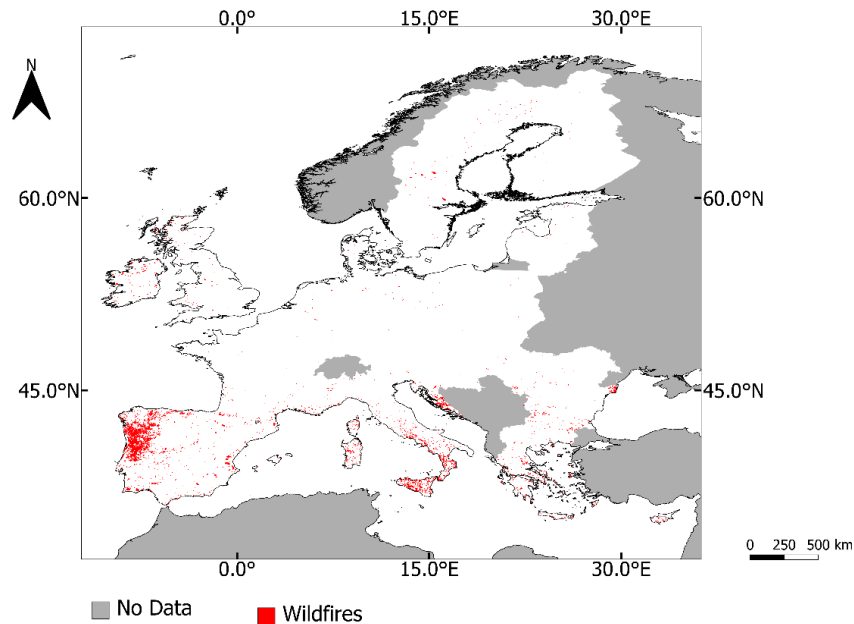
Figure 2. Wildfires in Europe from 2010 to 2018 larger than 10ha

Table 1. Number of wildfires per year

Year	2010	2011	2012	2013	2014	2015	2016	2017	2018
Number of fires	565	1088	1054	656	260	483	766	1907	716

Table 2. Classification of the wildfires by burned area.

Burned areas (ha)	Number of fires	Percentage (%)
10-100	3622	48,33
100-1,000	3387	45,19
1,000-10,000	462	6,16
>10,000	24	0,32
Total	7496	100

In In order to obtain information about the conditions before fires occurred, the following datasets have been added to the database: soil moisture (SM), land surface temperature (LST), wind speed (W), ecoregions (ER), land covers (LC), and the month of burning (M).

Soil moisture data is derived from the SMOS satellite ascending passes (6 a.m.). The product used for this study is the L4 with a resolution of 1 km (BEC, 2018). As an example, Figure 3 shows the mean moisture in Europe for the months of June during the study period.
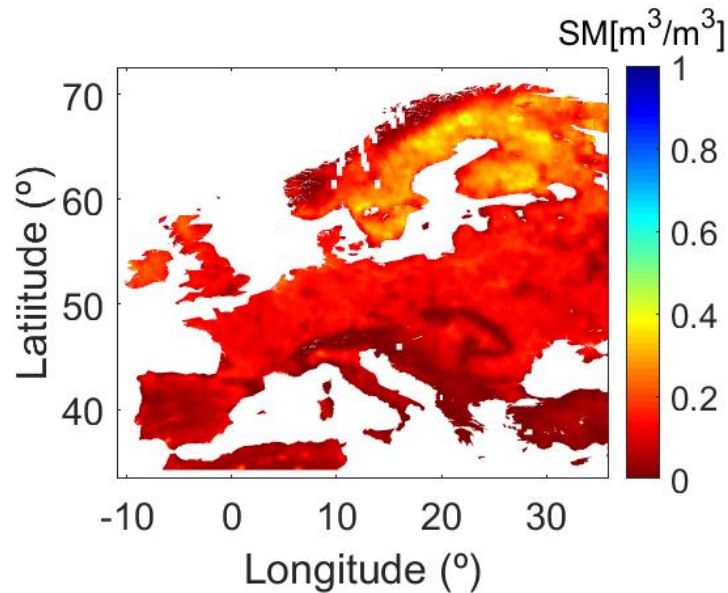
Figure 3. Mean soil moisture for the months of June during the period 2010 to 2018. Data at 1 km resolution from SMOS - L4 product (BEC, 2018).

Land surface temperature (LST) at midday is obtained from the ERA5 dataset of climatic reanalysed data (Albergel et al., 2018; ERA5-LST) provided by the European Centre for Medium-Range Weather Forecasts (ECMWF). Its resolution is approximately of 31km. In order to match the resolution of the SM dataset, the LST has been linearly interpolated to the SMOS L4 1km grid.
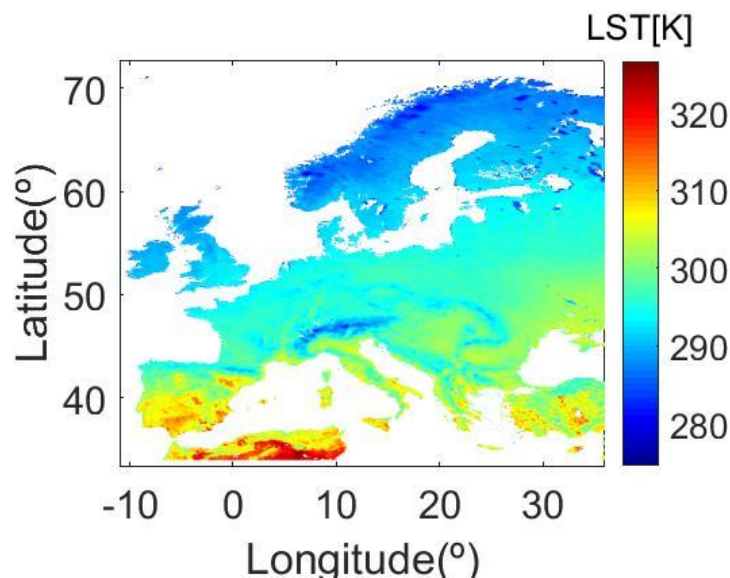
Figure 4. Mean land surface temperature for the months of June during the period 2010 to 2018, from ERA5 (ERA5-LST).

14

Wind speed (W) is obtained from the system UERRA-HARMONIE (UERRA. (2019)), it is provided in different height levels, and the 15 m height data have been used in this study. Its resolution is approximately of 11 km. It is worth noting that wind information was included as a complementary variable in order to explore its relationship with fire propagation, not being a factor included in the models.
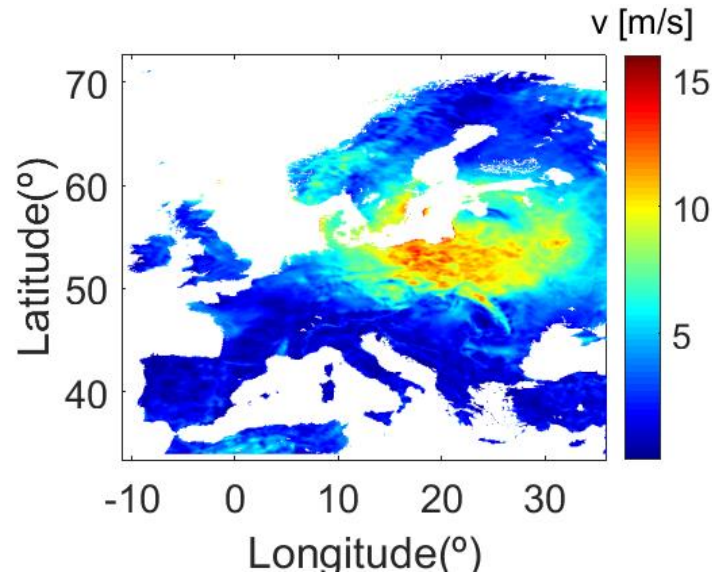
Figure 5. European wind speed map (1st January 2011; UERRA. (2019))

Figure 6 shows the land cover map used and which has been obtained from the CORINE (Bossard et al., 2000; *LAND COVER*. (2019) and allows classifying the fires depending on the type of vegetation burned. The CORINE land cover has a resolution of 250m and provides 44 categories of land cover classified in 5 groups: artificial surfaces, agricultural areas, forest and semi-natural areas, wetlands, and water bodies.
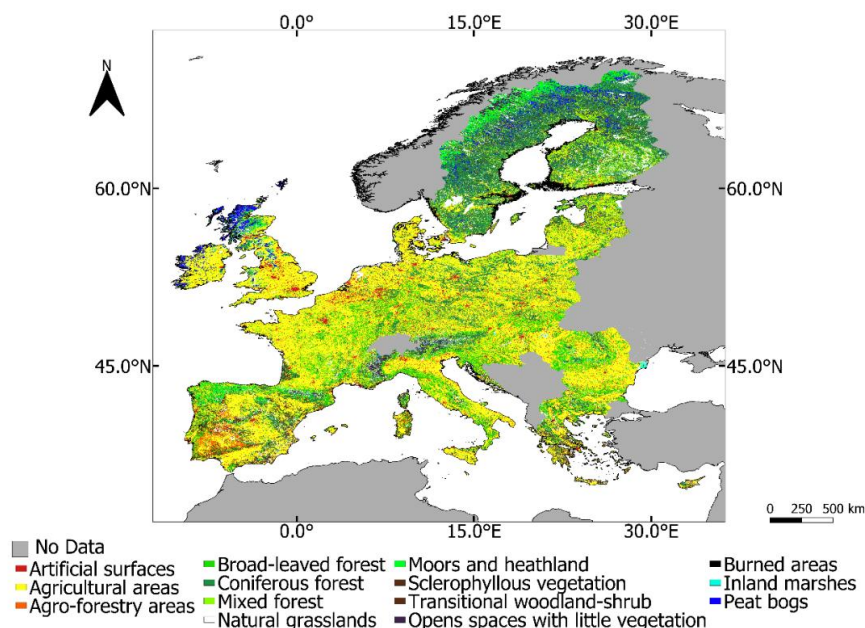
Figure 6. Land cover in the European Union, derived from the CORINE land cover map (LAND COVER.).

Ecoregions (ER, Metzger, 2005) have been used to classify fire locations in relatively homogeneous regions in terms of their climate, soil, and vegetation. This dataset divides Europe in 12 regions: Alpine North, Boreal, Nemoral, Atlantic North, Alpine South, Continental, Atlantic Central, Pannonian-Pontic, Lusitanian, Mediterranean Mountains, Mediterranean North and Mediterranean South (Figure 7).
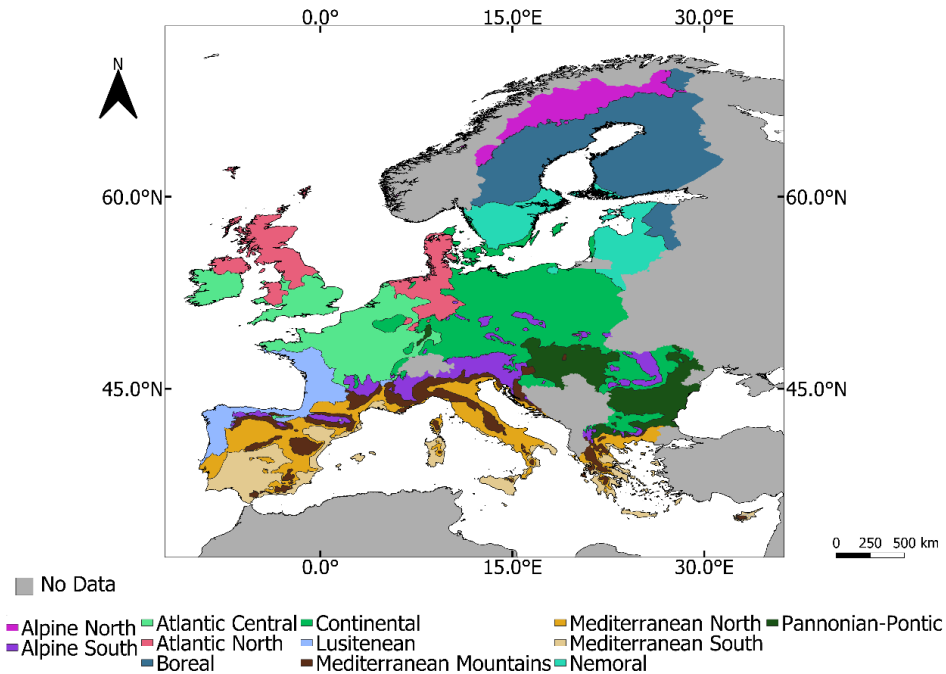
Figure 7. Ecoregions in the European Union.

2.2. Study area

The study area is the European Union (73.33ºN, 31.36ºN; -12.29ºW, 35.04ºW; excluding Madeira, Azores and Canary Islands) and it spans through more than 10 million km². As Europe is a vast continent, it presents contrasting climate patterns which determine the vegetation types and abundance, and consequently the fire ignition and spread. Figure 8 shows different temperature and precipitation regimes in Europe, with cold northern and Atlantic zones, continental regions with marked seasonal contrasts, and the hot and dry Mediterranean basin. Typically, in the north, as it is a subarctic region, the climate is defined by long and very cold winters, and short, cool to mild summers (Metzger et al.; 2012). The European mountainous regions, the inner continental lands, and the Pannonian-Pontic zones, present a continental climate, with a significant annual variation in temperature: hot summers contrast with very cold winters. Concerning to the Atlantic Central zone, it includes the south west and south of the British Islands, Northern France and the Netherlands: the climate is typically oceanic in the west, with cool wet winters and mild moist summers, but becomes more continental in the east (Metzger et al.; 2012). In the southern part of Europe there are two main regions: the Lusitanian and the Mediterranean. The Lusitanian zone includes west and south west France, northern Spain, and most of Portugal. The climate is warm and wet, with precipitation concentrated in the winter months. The

16

Mediterranean zones present warm and dry summers and precipitation concentrated in the autumn months (Metzger et al.; 2012).

The wet climate of the Lusitanian region leads to a high amount of fuel, which in warm conditions (especially in summer, in southern countries such as Portugal) brings to dangerous prone to fire conditions: more than one third of fires (37.66%) burn in this region. Also, the warm temperatures in the Mediterranean regions lead to almost 40% of fires burning in these areas (specifically, 19.58% burn in the Mediterranean South region, and 19.63% in the Mediterranean North region). In other areas, wildfires are less frequent such as in the case of Alpine North, Boreal and Nemoral regions, which are colder. However, exceptional dry and warm conditions have led to important burning episodes in countries such as Sweden or the United Kingdom in summer 2018 (Table 3).

Figures 8 and 9 present the prior conditions to the fire occurrences in terms of soil moisture and land surface temperature in relation to the ecoregion and land cover. The land covers transitional woodland-shrub, sclerophyllous vegetation, broad-leaved forest and agricultural areas presented the lowest values of soil moisture, while peat bogs, coniferous forest and inland marshes, the highest humidity values. Regarding regions such as Alpine south, Lusitanian, and Mediterranean zones registered the lower moisture values and also the warmest temperatures. There is a link between the wildfires in the regions with lower values of soil moisture and higher temperatures.

Figures 8 and 9 are coherent with Tables 3 and 4, showing that in regions where most wildfires occurred the temperatures were high and the soils were dry (i.e., in Lusitanian and Mediterranean regions). Concerning to land cover, transitional woodland-shrub and agricultural areas presented similar relationships.
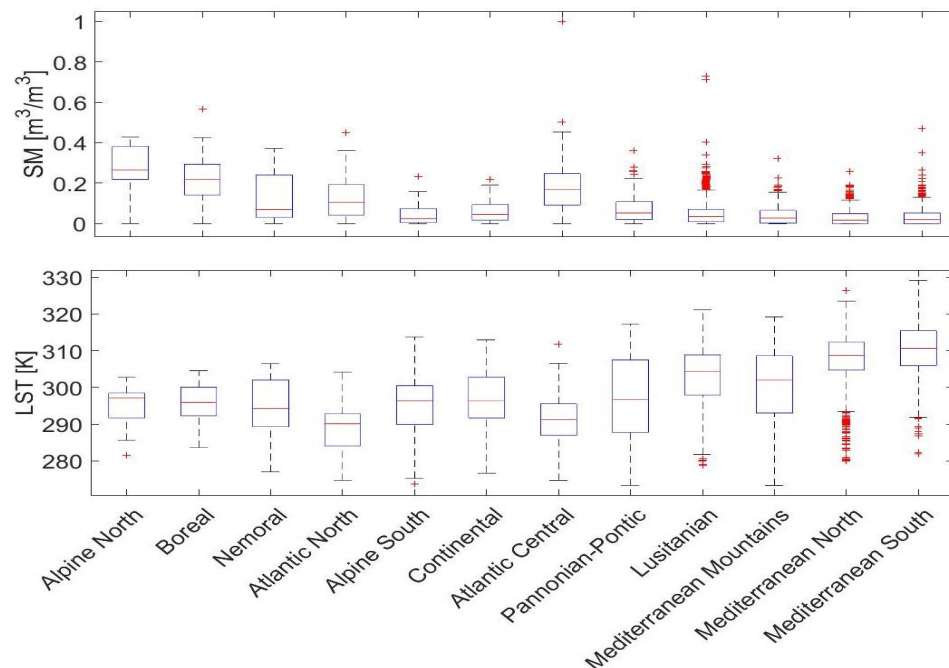
Figure 8. Relationship between temperature (top) and moisture (bottom) with ecoregions where fires burned.
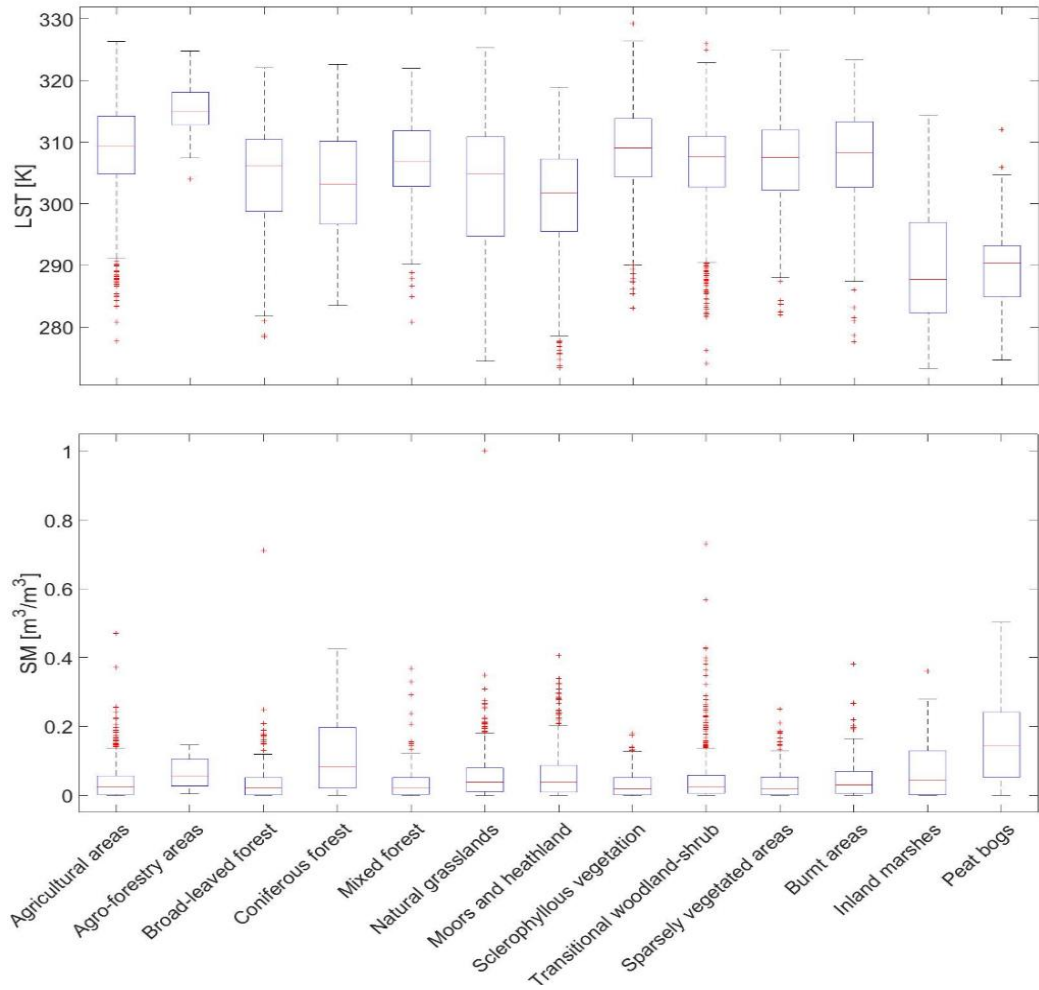
Figure 9. Relationship between temperature (top) and moisture (bottom) with land covers where fires burned.

Table 3. Wildfires classified by ecoregion.

Ecoregion Classification	Number of wildfires	Percentage (%)
Alpine North	17	0,23
Boreal	89	1,19
Nemoral	25	0,33
Atlantic North	203	2,71
Alpine South	211	2,82
Continental	111	1,48
Atlantic Central	112	1,49
Pannonian-Pontic	208	2,78
Lusitanian	2579	34,41
Mediterranean Mountains	528	7,04
Mediterranean North	1684	22,47
Mediterranean South	1728	23,06

In relation to fires distribution among land cover types, most fires occurred in moors and heathland, transitional woodland-shrub areas, agricultural areas, and grasslands. These four classes represent 67% of the total amount of wildfires registered (Table 4).

Table 4. Wildfires classified by land cover.

Land cover classification	Number of wildfires	Percentage (%)
Agricultural areas	1223	16,32
Agro-forestry areas	22	0,29
Broad-leaved forest	467	6,23
Coniferous forest	218	2,91
Mixed forest	163	2,17
Natural grasslands	729	9,73
Moors and heathland	1721	22,96
Sclerophyllous vegetation	608	8,11
Transitional woodland-shrub	1356	18,09
Sparsely vegetated areas	513	6,84
Burnt areas	218	2,91
Inland marshes	97	1,29
Peat bogs	161	2,15

Finally, note that most wildfires (4,322 out of 7,495) burned in summer months (i.e., June, July and August, Table 5).

Table 5. Number of wildfires by month.

Month	Jan.	Feb.	March	April	May	June	July	Aug.	Sep.	Oct.	Nov.	Dec.
Number of wildfires	48	169	504	399	241	488	1492	2342	876	791	75	70
Percentage (%)	0,64	2,25	6,72	5,32	3,22	6,51	19,91	31,25	11,69	10,55	1,00	0,93

2.3. Database

In order to build the database used in this study, firstly the 7569 wildfires have been classified in terms of land cover, ecoregion, soil moisture and land surface temperature. To that purpose, the geographic positions of the burned pixels have been linked to all data maps using the minimum distance between the centres of the pixels. For each fire, the ER and LC modal class among the affected pixels has been computed. For quantitative variables (LST and SM) the mean has been computed. Note that SM and LST data from the day of fire occurrence to three days before have been included in the database. The most recent data available has been used (although finally information from the date of fire occurrence has been omitted due to operational limitations; see Section 2.4).

After that they were filtered under certain conditions, so from the initial data of 7569 wildfires, to the final dataset composed by 7496 fires, as said before, fires in the islands and fires before July 2010 were eliminated; then some land covers were not considered (artificial surfaces, maritime wetlands

water bodies and open spaces with little or no vegetation), because this study will focus only in forest wildfires so 23 wildfires were removed from the dataset.

2.4. Development of a model to predict the potential extension of wildfires

Since the goal of this work is to develop a model to predict the potential extension of wildfires, in this section several models will be presented and compared. The different models tested are ordered in this section from the simplest to the most complex. These models are essentially based on the SMOS-derived soil moisture and on the ERA5 land surface temperature, but also explore the influence of the land cover, the ecoregions, and the time of fire burnings.

However, as a previous step to the model development, the availability of data for operational purposes must be considered. In that sense, data of LST for the day of fire ignition at noon cannot be used to produce operational propagation risk maps for obvious reasons: most fires burn during morning and at noon, so risk maps could not reach the fire prevention services on time. Also, it must be considered that L4 SM products from ascending passes are not available the same day of data acquisition. Additionally, the possibility of acquiring LST forecasts for the study day is not affordable on economic terms (as such data is delivered after payment to the Spanish meteorological agency, AEMET, on behalf of ECMWF). For these reasons, model calibration has been based on the most recent SM and LST data from the day previous to fire occurrences to three days before. To evaluate the differences between the fire date and the day before fire burning, LST and SM have been compared for both cases. Results are shown in Figure 10 and demonstrate that mean differences peak is approximately at zero. Hence, similarities between both days suggest that moisture and temperature data for days before fires can be used for model calibration.
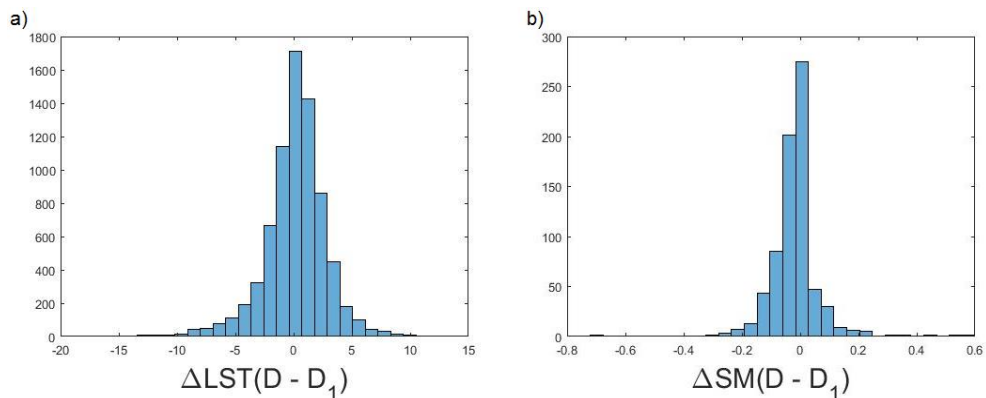

Figure 10. Differences between the fire date and one day before fires for (a) land surface temperature and (b) soil moisture.

2.4.1. Preliminary analysis of SM and LST relationship with wildfires propagation

To build the model 70% of the registered fires (training dataset) have been used. The remaining 30% has been used for validation purposes (validation dataset). The distribution in these two groups have been done with a random sample. Soil moisture and temperature of the training set are plotted against burned area, which has been logarithmically transformed (decimal logarithm), following Chaparro et al. (2016a) and Chaparro (2018). Figure 11 shows the resulting triangle shaped plots, where both moisture and temperature limit the fire extent.
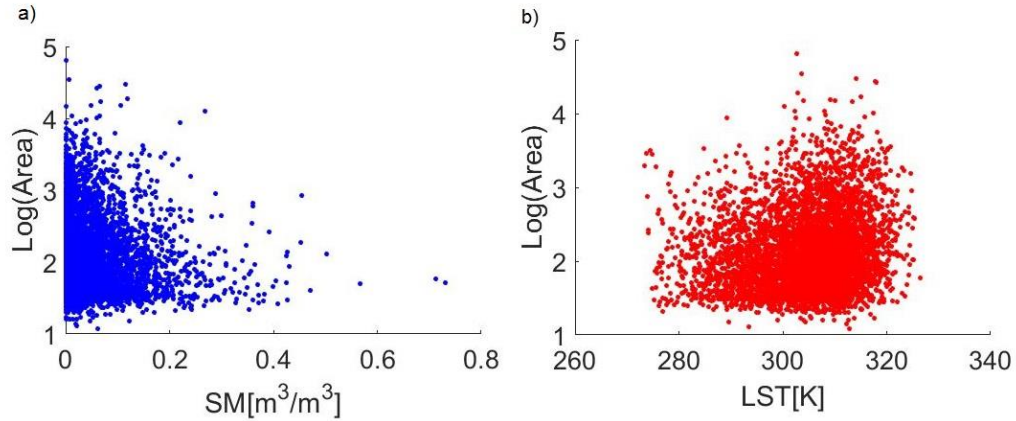
Figure 11. Decimal logarithm of burned area (originally in hectares) for the training dataset is plotted against (a) soil moisture and (b) land surface temperature.

From the previous plots, an "imaginary hypotenuse" of each triangle delimits the maximum burned area at different values of SM or LST. Hence, higher temperatures lead to larger burned areas, and drier soils are linked, also, with larger wildfires. Obviously, multiple factors (e.g., extinction capacity, lack of fuel, changing meteorological conditions…) lead in most cases to smaller fires than which could be expected from the SM and LST conditions. Hence, the approximation based on triangular-shaped relationships between moisture, temperature, and burned area pursues to predict the maximum or potential propagation of fires at particular SM and/or LST conditions, using a linear regression to approximate the hypotenuse of the triangle. To this purpose, the variables SM and LST have been binned, and the largest fires for each bin have been chosen in order to fit these linear regressions. This method has been used previously in Chaparro et al. (2016a) for the Iberian Peninsula. Different modelling approaches have been tested and are described hereafter:

2.4.2. SM-burned area and LST-burned area models

Different SM and LST bins have been tested: from 0.01 m³/m³ to 0.05 m³/m³, and from 1K to 4 K, respectively. Firstly, a linear regression to estimate Log(Area) has been performed as a function of SM (Eq. 2.1.):

$$Log_{10}(Area) = \alpha_{SM} + \beta_{SM} \cdot SM, \qquad (2.1)$$

where $Log_{10}(Area)$ corresponds to the maximum of the decimal logarithm of burned area for each SM bin, α_{SM} is the intercept, SM is soil moisture, and its coefficient is β_{SM}.

The same approach has been used for LST:

$$Log_{10}(Area) = \alpha_{LST} + \beta_{LST} \cdot LST \, , \qquad (2.2)$$

where $Log_{10}(Area)$ corresponds to the maximum of the decimal logarithm of burned area for each LST bin , α_{LST} is the intercept, LST is the land surface temperature, and its coefficient is β_{LST}. Samples for models 2.1 and 2.2 are 47 and 48 fires, respectively, in the case of the binnings chosen (see Section 3.1).

After such models have been tested, an important number of wildfires exceed the potential propagation predicted (see Section 3.1). To solve this underestimation, an additive factor (equivalent to one standard deviation of LogArea) was added to the intercept of both equations. Then, Eqs. 2.1 and 2.2 changed to:

$$Log_{10}(Area) = \alpha'_{SM} + \beta \cdot SM \, , \qquad (2.3)$$
$$Log_{10}(Area) = \alpha'_{LST} + \beta \cdot LST \, , \qquad (2.4)$$

where:

$$\alpha'_{SM} = \alpha_{SM} + \sigma_{\log(area)} \text{ and } \alpha'_{LST} = \alpha_{LST} + \sigma_{\log(area)\prime}$$

$$\sigma_{\log(area)} = 0,9396$$

$$\sigma_{\log(area)\prime} = 0,5013$$

These regressions are parallel to Eqs. 2.1 and 2.2 (i.e., same slope), but represent more reliably the maximum extension of fires at each SM or LST value.

2.4.3. Models combining SM and LST

After analysing the relationships Log(Area)-SM and Log(Area)-LST, a second step consisted on applying both variables in the same model. The same procedure (i.e., binning the variables) has been applied. However, now the variables have been binned together: soil moisture bins are 0.01 m³/m³, 0.02 m³/m³ and 0.03 m³/m³ and LST bins are 1K, 2K and 3K. All combinations of SM-LST bins have been tested. In this case, the equation linking SM and LST to the burned area is:

$$Log_{10}(Area) = \alpha + \beta \cdot SM + \gamma \cdot LST, \qquad (2.5)$$

where $Log_{10}(Area)$ corresponds to the largest (over 90th percentile) decimal logarithm of burned area per each SM-LST bin, α is the intercept, SM is the soil moisture, LST is the land surface temperature, and their coefficients are β and γ, respectively. The sample for this equation using the binning which provides the best fit (see Section 3.1) is 639.

As an attempt to improve Eq. (2.5), the model has been finally complemented with auxiliary variables: land cover, ecoregions, and the month when the wildfire burned. Only those variables and those interactions which are significant at 95% confidence level (p<0.05) have been chosen and included in the model defined by Eq. (2.6):

$$Log_{10}(Area) = \alpha + \beta_{(M,LC)} \cdot SM + \gamma_{(ER,LC)} \cdot LST + M + LC + ER, \qquad (2.6)$$

where $Log_{10}(Area)$ corresponds to the largest (over 90th percentile) decimal logarithm of burned area per each SM-LST bin , α is the intercept, SM is the soil moisture, LST is the land surface temperature, M refers to the moth of the wildfire, LC refers to the land cover classification, ER refers to the ecoregion and the coefficients are: $\beta_{(M,LC)}$ for SM (which changes depending on the interaction with month and land cover) and $\gamma_{(ER,LC)}$ for LST (which changes depending on the interaction with ecoregion and land cover).

In this model, the classification of ecoregions has been changed from that in section 2.1 in order to fit the best model and to reach enough sample in each area. The best reclassification is found when grouping the original ecoregions in three large areas as follows:

1. North: Alpine North, Boreal and Nemoral.
2. Central: Atlantic North, Alpine South, Continental and Atlantic Central.
3. South: Alpine South, Pannonian-Pontic, Lusitanian, Mediterranean Mountains, Mediterranean North and Mediterranean South.

In addition, agricultural areas and agro-forestry areas have been grouped also in a single category to ensure enough sample in this group.

2.4.4. Validation of the models and development of potential fire propagation maps

The models applied have been validated using the validation dataset. To this purpose, the burned area of each wildfire has been estimated using the different models, and compared to the real value of fire extent. Validations for the different models have been compared in order to choose the best model. Then, this model has been used to provide European maps of potential fire propagation. The best solution is presented at results section.

2.4.5. Relationship between wind and burned area

The influence of the wind in the wildfire propagation has been also studied since it is an important factor which usually increases the fire spread, turning extinction tasks difficult. This task has been performed with exploratory purposes using part of the dataset (specifically fires between June 2010 and December 2013).

3. Results

3.1. SM-burned area and LST-burned area models

Fitting for models in Eqs. 2.1 and 2.2 changes depending on the bin width chosen. After analysing results with several binnings, it has been decided to select the smallest bin since bigger bins excessively reduce the sample (n<20). So, for Eq. (2.1) the binning chosen is ΔSM = 0.01 m³/m³ and for Eq. (2.2) it is ΔLST = 1 K. Table 6 shows goodness of fit and sample for these models.

Table 6. Bin widths for SM and LST.

	Δ (bin width)	R²	Sample
Δ SM [m³/m³]	0,01	0,73	47
Δ LST [K]	1	0,40	48

The regression between the logarithm of burned area and soil moisture is presented in Figure 12, which represents the models described by Eqs. 2.1 and 2.3.
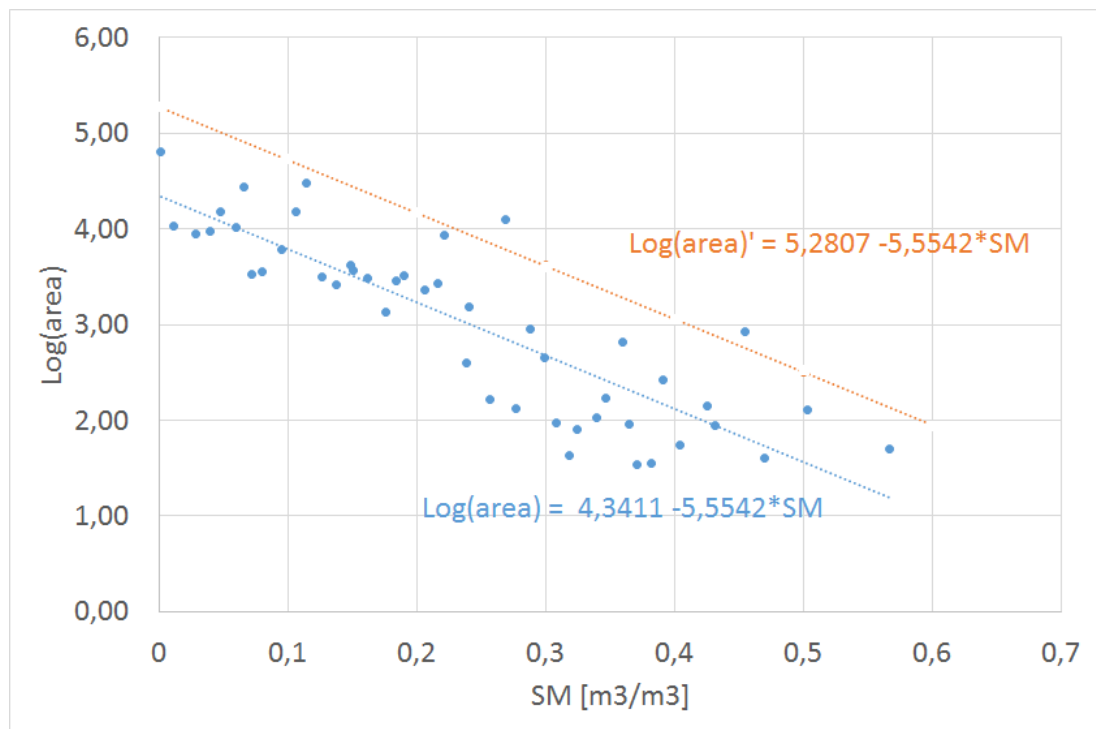

Figure 12. Regressions of LogArea as a function of SM for Eq. 2.1 (blue) and 2.3 (orange).

The relationship between the logarithm of burned area and the land surface temperature is presented in Figure 13, both for Eq. 2.2 and for Eq. 2.4.
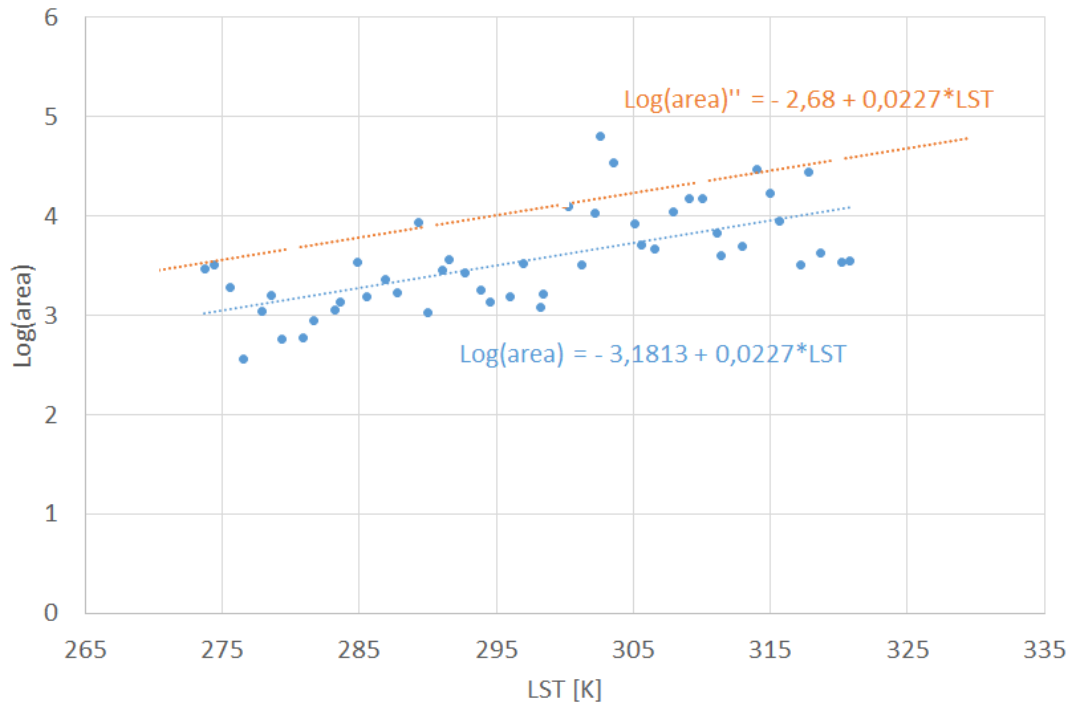
Figure 13. Regressions of LogArea as a function of LST, both for Eq. 2.2. (blue) and 2.4 (orange).

3.2. Models combining SM and LST

The linear regression proposed by Eq. 2.5 applies SM and LST as explanatory variables. The best model in terms of R^2 has been chosen from the different binning possibilities reported in Table 7.

Table 7. R^2 values for different bins of SM and LST in Eq. 2.5. Bold font highlights the binning finally chosen for the SM-LST model.

ΔLST [K] / ΔSM [m³/m³]	1	2	3
0,01	0,37	0,45	**0,48**
0,02	0,45	0,47	0,45
0,03	0,47	0,46	0,43

The best regression has been obtained for the combination ΔLST = 3K and ΔSM= 0.01 m³/m³, with a R^2 = 0,48 (p<0.0001). LST and SM range from 274 to 321 K and from 0 to 0.57 m³/m³, respectively. The relationship between these variables and LogArea is shown in Figure 14, where the largest fires are generally found in the driest and warmest soils. For instance, most of the bins with maximum spread ≥1,000 ha (i.e., $Log_{10}(Area)$≥ 3) present SM≤0.10 m³ /m³ and LST≥300 K. Finally, coefficients α, β and γ for the Eq. 2.5 are -3,331, -2,708 and 0,0193, respectively.
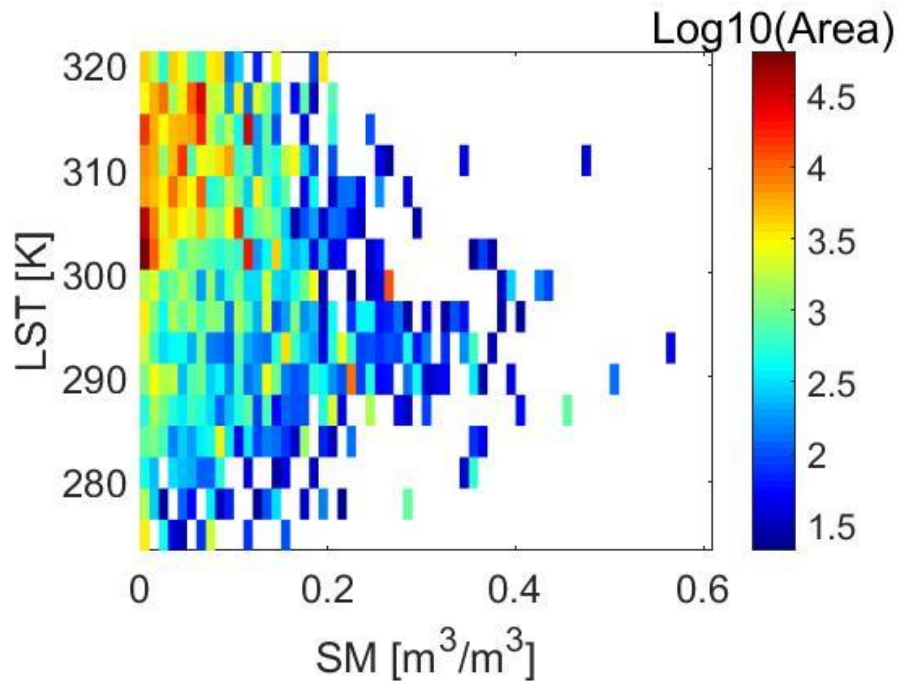
Figure 14. Relationship among SM, LST and the percentile 90 of the decimal logarithm of burned area (colorbar) for each SM-LST bin. Binning: $\Delta LST = 3K$ and $\Delta SM = 0.01$ m^3/m^3. This binning led to the model in Eq. 2.5, with $R^2 = 0.48$.

Finally, the last model proposed (Eq. 2.6) includes: SM, LST, the month of fire occurrence, the land cover, the ecoregion, and the interactions SM × month, SM × land cover, LST × land cover, and LST × ecoregion. A detailed description of the sample is reported in Table A1 in the Appendix.

The adjusted R^2 of the model is 0,57. The variance explained by this model is reported in Table 8, showing that SM was the variable explaining most of the variance (25%), followed by LST (24%).

Table 8. Variance explained by each variable in Eq. 2.6. The variance explained by the model is 0,61 ($R^2=0.61$). Nevertheless, the adjusted R^2 (0,57) is used hereafter as it is unaffected by possible redundancy of information.

Variable	Variance model (%)	Variance total (%)
LST	38,83	23,74
SM	41,01	25,08
M	3,78	2,31
LC	5,24	3,21
ER	0,03	0,02
SM×M	4,21	2,58
SM×LC	4,12	2,52
LST×LC	1,62	0,99
LST×ER	1,15	0,70
Total	100,00	61,15

Figures 15, 16, 17, 18 and 19 show the prediction of burned area as a function of land surface temperature, soil moisture, month, region and land cover. The potential propagations predicted report how SM and LST limit the maximum burned area (Figures 15 and 16) up to a maximum of ~3100 ha. Months with more predicted burned areas are July, August, September and October. Months with less predicted burned areas are February, November and December (Figure 17). This is information coherent with data from the Table 5 (Section 2.2.). The south of Europe is the region where the largest wildfires are predicted (Figure 18). Wildfires in land covers like broad-leaved forests, moors and wetlands, transitional woodland-shrub and burned areas have a prediction to burn larger fires. In contrast, mixed forests, inland forest and coniferous forests have a prediction to burn smaller areas (Figure 19).

Figure 15. Prediction of the decimal logarithm of burned area (originally in hectares) for the model described by Eq. 2.6, plotted against land surface temperature. Note: Log(area)* corresponds to the predicted area.

Figure 16. Prediction of the decimal logarithm of burned area (originally in hectares) for the model described by Eq. 2.6, plotted against soil moisture. Note: Log(area)* corresponds to the predicted area.

Figure 17. Prediction of the decimal logarithm of burned area (originally in hectares) for the model described by Eq. 2.6, plotted against the months, Note: Log(area)* corresponds to the predicted area.

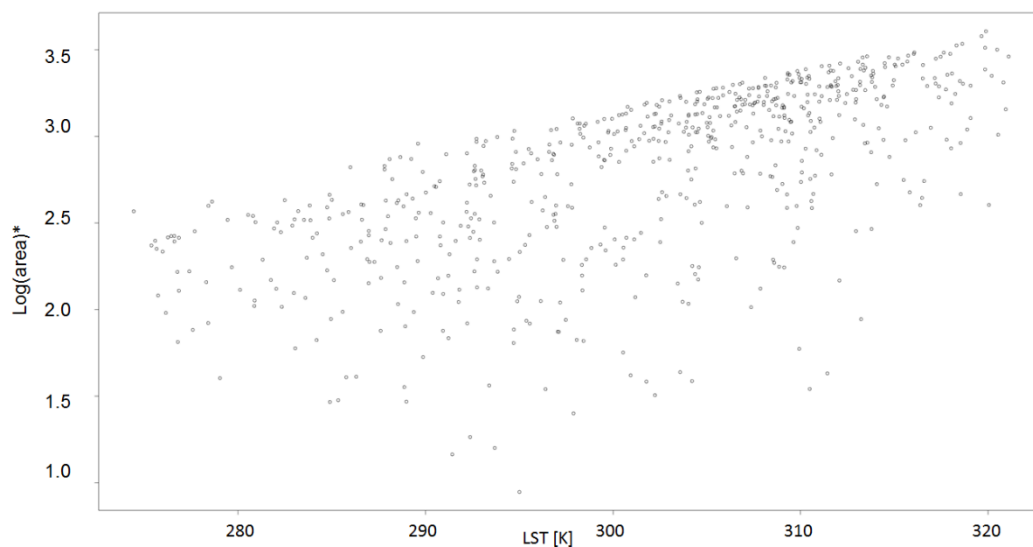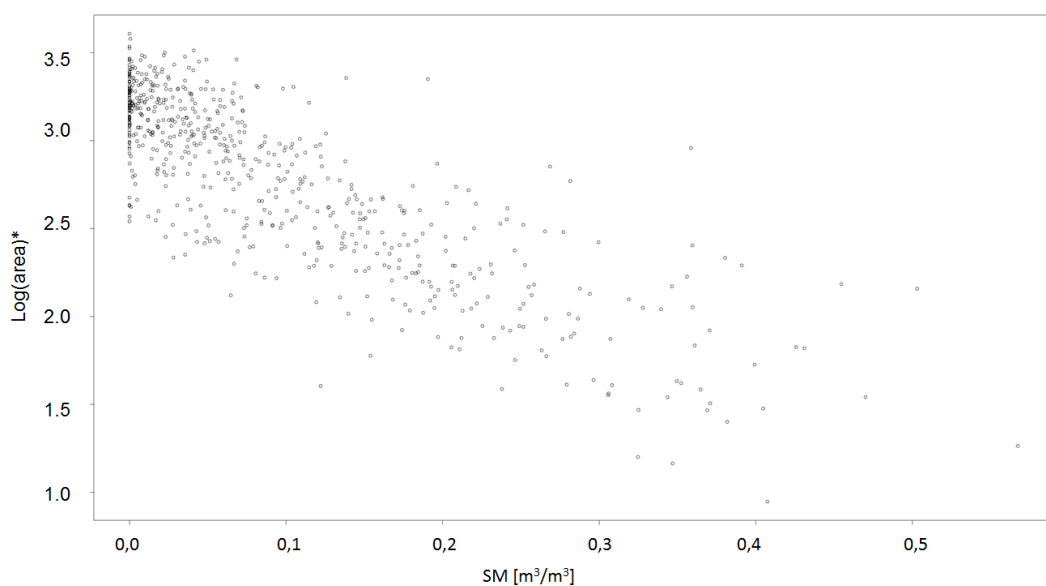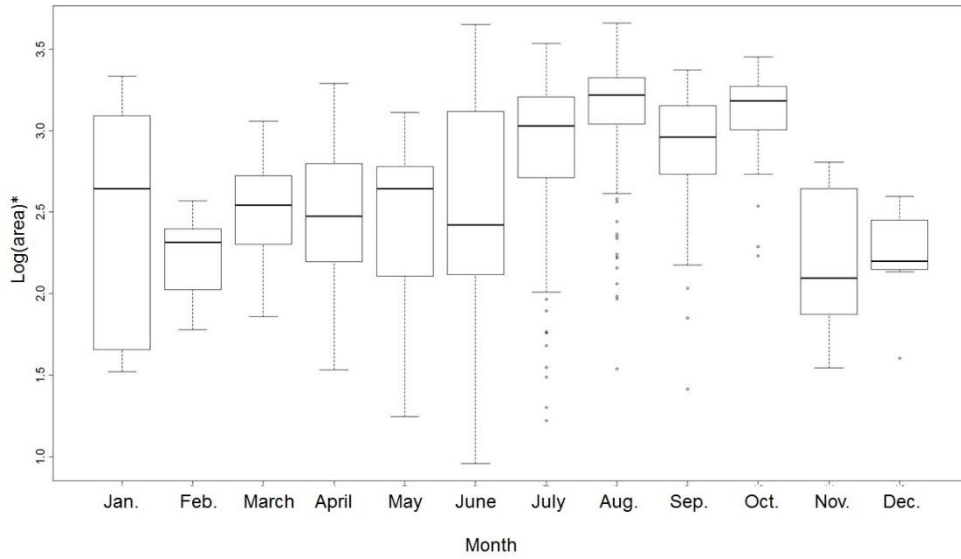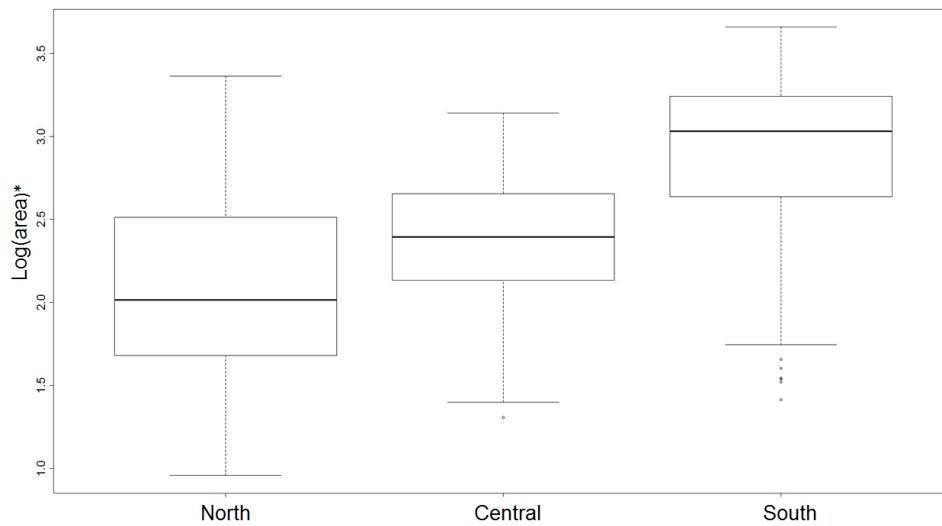**Figure 18** Prediction of the decimal logarithm of burned area (originally in hectares) for the model described by Eq. 2.6, plotted the ecoregions. Note: Log(area)* corresponds to the predicted area.
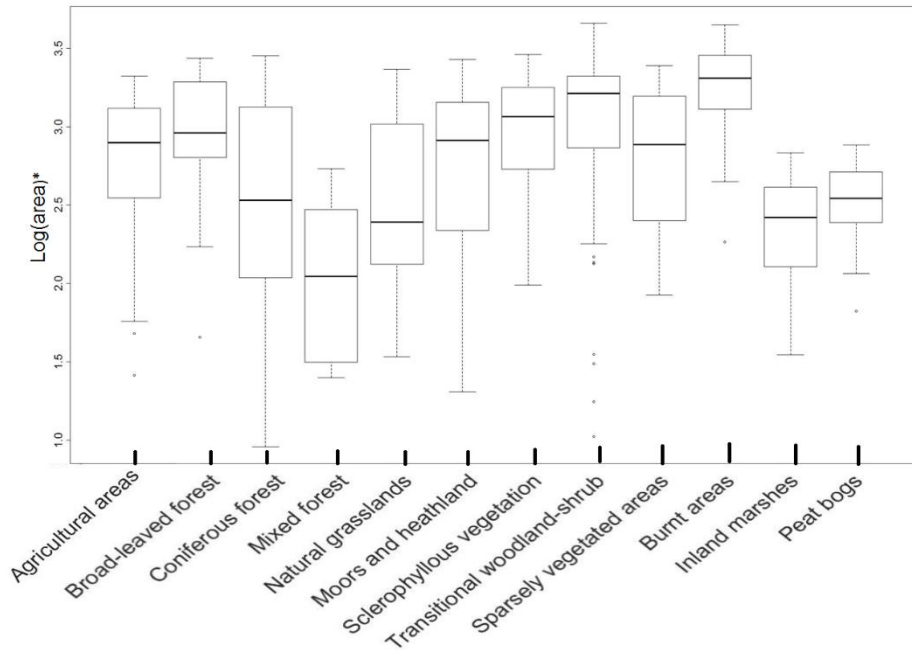
Figure 19. Prediction of the burned area in relation to the land cover. Note: Log(area)* corresponds to the predicted area.

Figures 20, 21, 22 and 23 show the interactions between the variables. The interactions between the temperature and the different regions are shown in Figure 20, where the slope is larger in the northern region showing larger impact of temperature in this area. Concerning LST and SM interactions with land cover (Figure 21 and 22), most effects of these variables are consistent with the overall pattern (i.e., higher risk in warmer and drier conditions). Nevertheless, some exceptions are found: (i) mixed forests present an opposite effect (although with wide confidence intervals probably due to low sample); (ii) an almost flat trend is found in humid land covers (inland marshes and peat bogs); and (iii) broadleaved forests do not show a clear trend for SM (Figures 21 and 22). Concerning to the SM × months interaction, a coherent pattern is found for most months (Figure 23).
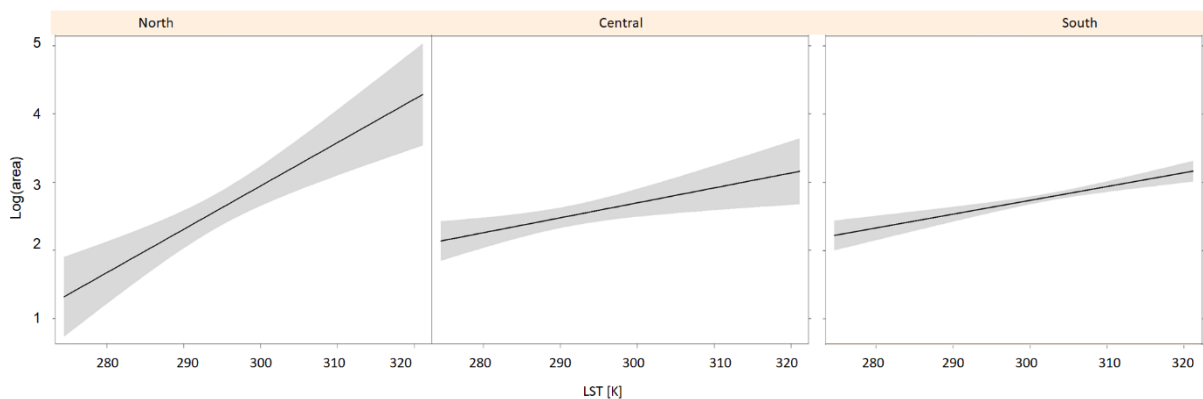
Figure 20. Interaction between land surface temperature and ecoregions, plotted as function of the decimal logarithm of burned area (originally in hectares) from the model described by Eq. 2.6.

29
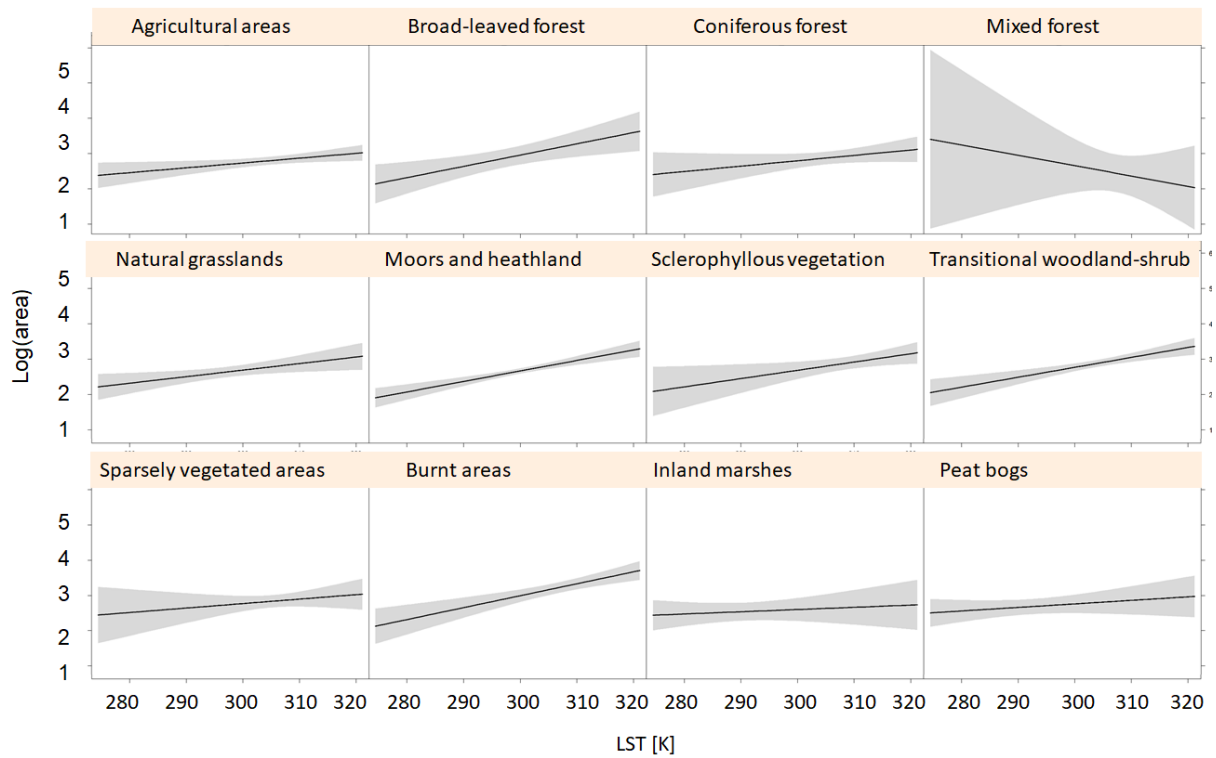
Figure 21. Interaction between land surface temperature and land cover, plotted as function of the decimal logarithm of burned area (originally in hectares) from the model described by Eq. 2.6.
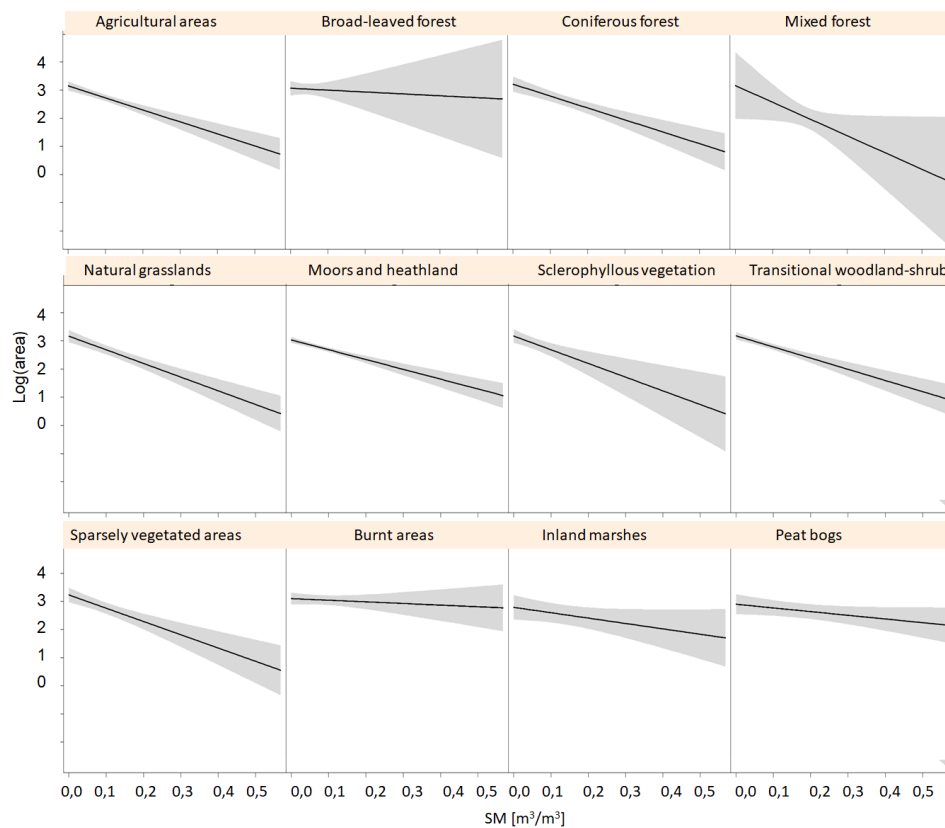
Figure 22. Interaction between soil moisture and land cover, plotted as function of the decimal logarithm of burned area (originally in hectares) from the model described by Eq. 2.6.

30
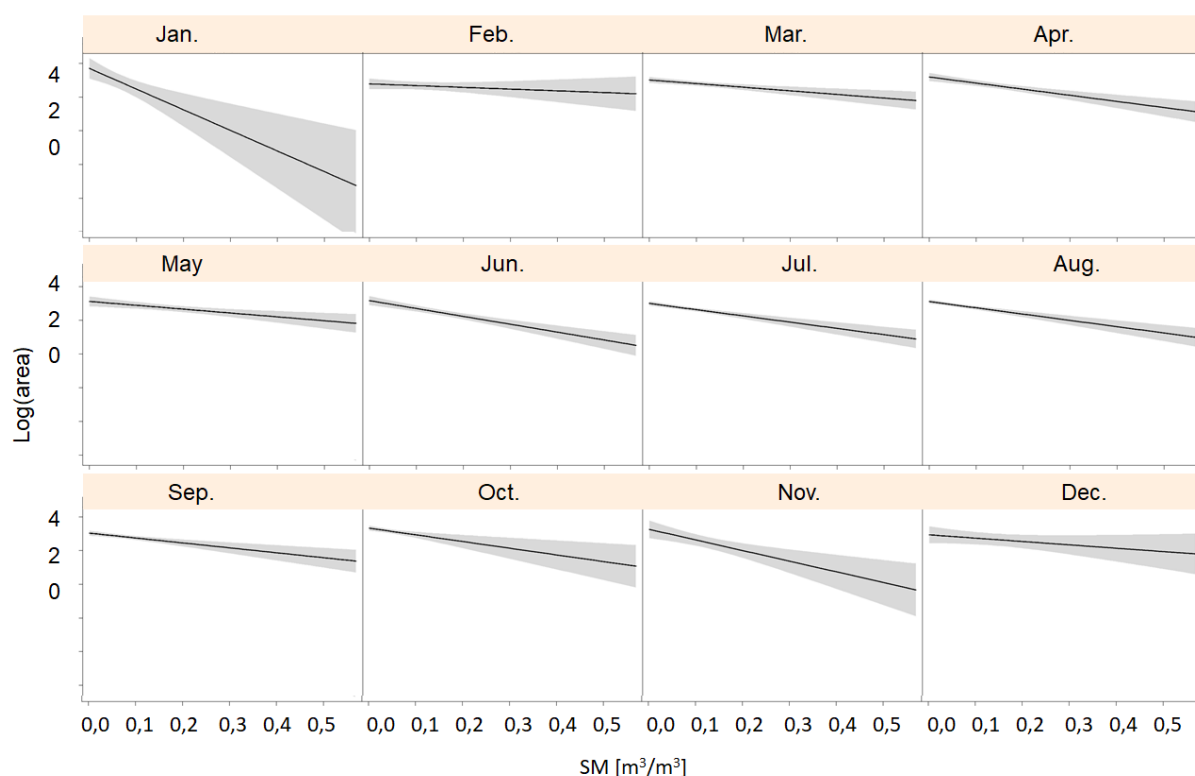
Figure 23. Interaction between soil moisture and month, plotted as function of the decimal logarithm of burned area (originally in hectares) from the model described by Eq. 2.6.

3.3. Summary of all models

All the models have been validated using the validation dataset. Results are shown in Table 9. Eq. 2.3 presents the lowest errors and will be applied for mapping potential fire propagation.

Table 9. Comparison between all models. *Note: Models 2.3 and 2.4 are similar to 2.1 and 2.2, respectively (same slope, but different intercept). Bold shows the model which will be finally applied.

Equation	R^2	Correct validation	Correct validation (%)	Max. excess (max. error) [ha]	Fires >10k ha [correctly classified] (%)	Fires >10k ha [incorrectly classified] (%)
2.1 - SM	0,73	1890	99,21%	27917,60	16,67	83,33
2.2 - LST	0,40	1885	90%	29773,69	0,00	100,00
2.3 – SM*	*	**1904**	**99,94%**	**215,15**	**100,00**	**0,00**
2.4 – LST*	*	1902	99,84%	18959,78	66,67	33,33
2.5 – SM & LST	0,48	1750	91,87	33520,91	0,00	100,00
2.6– SM & LST & interactions	0,57	1727	90,65	33655,11	0,00	100,00

3.4. Maps of predicted potential burned area

Results show how the suggested methodology provides good approximation to the maximum expected fire spread. In that sense, it is possible to obtain maps of predicted potential burned area based on the best model (Eq. 2.3). Figure 24 presents an example of these maps with the predicted maximum potential area being classified in different risk categories (Table 10).

Table 10. Classification of the predicted maximum potential burned area in the risk categories of Figure 24.

Predicted area (ha)	<100	100 - 1000	1000-10.000	10.000-50.000	>50.000
Risk category	Low	Moderate	High	Very high	Extreme
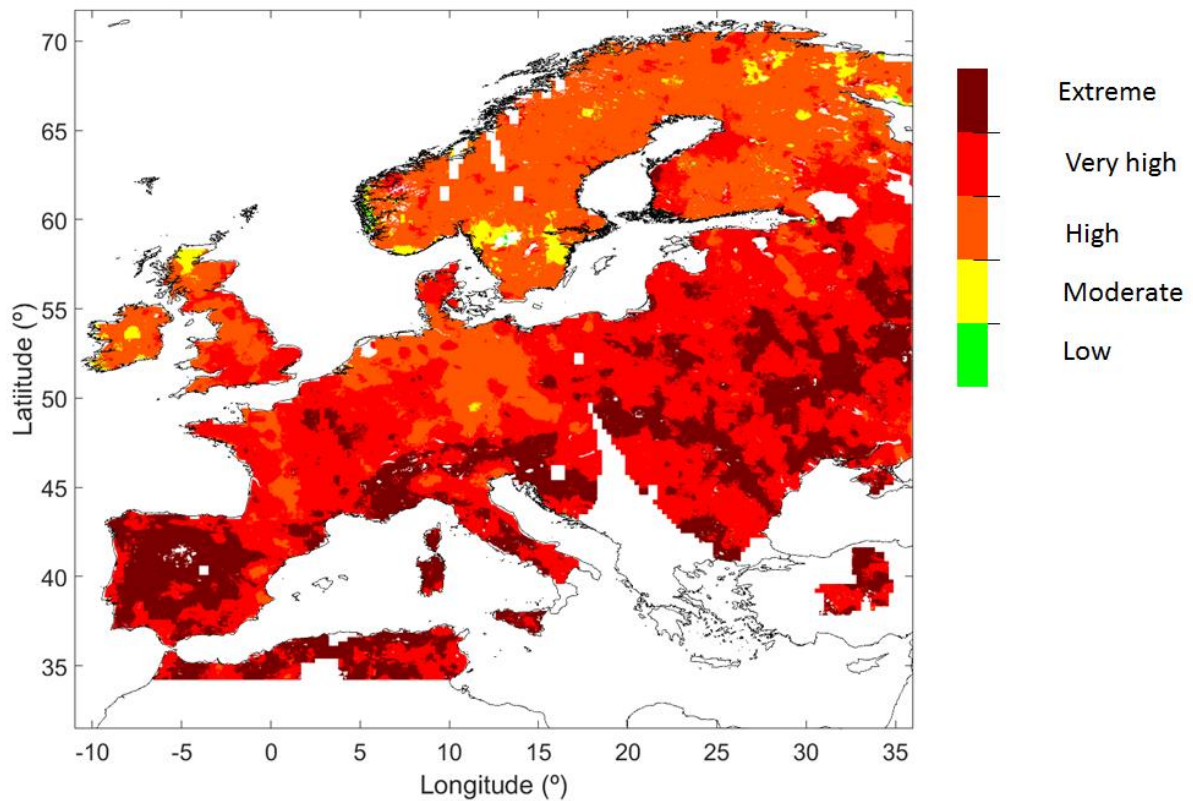
Figure 24. Example of a maximum potential area map (20th August 2015) derived from Eq. 2.3.

3.5. Wind influence

In this study the wind speed absolute value (no direction) has been considered. The effect of the absolute value of wind speed in wildfires propagation is plotted in Figure 25. It has been found scarce relationship between the wind speed absolute value and the logarithm of burned area ($R^2 = 0,03$). This is further discussed in Section 4.
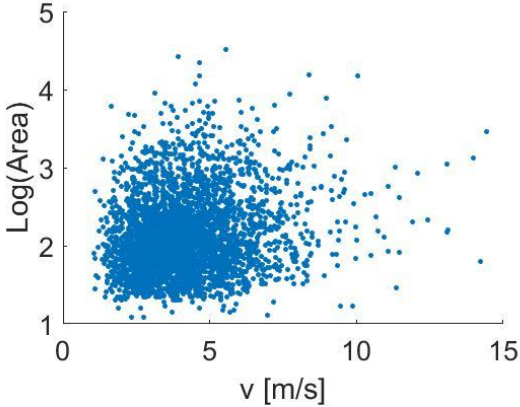
Figure 25. Decimal logarithm of burned area (originally in hectares) and wind speed for wildfires from 2010 to 2013.

4. Discussion

4.1. Role of soil moisture and land surface temperature in fire propagation

SMOS-derived soil moisture has been found to be an important explanatory variable in evaluating fire propagation in the European Union. Results show that wet soils strongly limit burned area and, in an opposite way, drier soils increase the potential risk of large forest fires. Concerning surface temperature, the largest wildfires happen under high temperatures, while propagation risk decreases in colder situations. These results are consistent with similar studies in the Iberian Peninsula (Chaparro et al., 2016 a, and b) and also in other regions of the world (Bartsch et al., 2009). There is a strong link between large burned areas, high temperatures and low values of soil moisture, and a large percentage of fires larger than >1000 ha have burned under these conditions (Figure 14). This results allow determining a maximum or potential burned area as a function of SM and/or LST, either used separately in specific models, or combined in a single regression. This approach has explained between 40% and 73% of the potential burned area (Table 10). This is coherent with previous models developed in the Iberian Peninsula (Chaparro et al., 2016a).

The model based on soil moisture (Eq. 2.3) has shown the best results once an additive factor (σLogArea) has been included ($R^2 = 0.73$; maximum error = 215 ha). Similarly, soil moisture has shown also important capacity to explain fire propagation (25% of explained variance; Eq. 2.6) when combined with LST. Concerning to LST, the variance explained by this variable is lower (40% in Eq. 2.2; 24% when combined with SM in Eq. 2.6). This effects are consistent with the research performed for the Iberian Peninsula by Chaparro et al. (2016 a, and b), where SM explained 33% and LST 20% of the modelled variance. However, the present results surprisingly report an improved performance of the simplest models (based on SM) if compared to the model combining SM and LST. In this case, we suggest that the scarce correlation found between SM and LST (r = -0.31) may explain that including both variables could add noise to our model. In particular, the relationship found in Figure 14 is not perfect and may be decoupled because, although large fires burn in high temperatures and dry soils, both LST and SM preceding these fires show important variability (approximately from 300 to 320 K and from 0 to 0.10 m^3/m^3 in the largest fires).

4.2. Land cover, ecoregions, and month of fire burning

Including complementary variables, such as land cover, ecoregions and month, and their interactions (Eq. 2.6) has led to a poor improvement ($R^2 = 0,57$) with respect to the basic SM-LST model (Eq. 2.5; $R^2 = 0,48$). There might be some reasons for that. Firstly, the application of the method used for the Iberian Peninsula in Chaparro et al. (2016a) might not be similar for the entire European Union (as it is a larger study area with many different contrasting patterns in terms of climate and vegetation). Secondly, the significance and applicability of the proposed variables may differ among regions of Europe and, importantly, maybe other variables than those tested in the Iberian Peninsula should be tested now (e.g., synoptic situations, fuel amount, vegetation indices, etc…). In that sense, the influence of the ecoregions is almost negligible when compared to the other variables (<1%), possibly due to the fact that SM and LST do capture most climate variability through the temperature and moisture gradients in the continent (see Metzger et al., 2005), leading ecoregions to be a redundant source of information.

In addition, the effect of land covers on fire propagation has shown some different patterns if compared to the land cover – burned area relationships found in Chaparro et al. (2016a). For example, the coniferous forests –which are very prone to large wildfires in the Iberian Peninsula- do show a large variability in predicted burned area in this study (see Figure 19). This is probably because very different coniferous forests exist in Europe, with great contrasts, for instance, between Mediterranean pines and boreal forests.

Although the aforementioned variables do not contribute importantly to the propagation fire risk assessment, most of their effects and interactions show coherent patterns. For instance, in northern regions the role of LST is more marked than in southern and warmer areas (Figure 20), similarly to what is reported in Chaparro et al. (2016a) for the Iberian Peninsula. Also, as expected, larger wildfires are predicted in the south of Europe rather in the north and central regions, which is coherent with the main climate patterns and with number of fires per region reported in Table 3. Regarding the months, the summer months (July, August), but some autumn months as well (September and October) present higher predicted burned areas.

4.3. Validation and application of a model to predict potential burned area

The model described by Eq. 2.3, which applies SM + σLogArea has been selected for operational applications. The validation shows an agreement of 99.94% with a maximum error of 215,15ha, and reports that no fires larger of 10,000 ha have been underestimated. It is important to note that this high accuracy is reached due to the addition of the σLogArea factor, which avoids underestimation of most fires. Although this could also lead to an overestimation, the intercept of the Eq. 2.3 ($\alpha = 5,28$) shows that the maximum fire propagation would be of ~100.000 ha. This is consistent with: (i) the largest fires detected in the EU during the study period (which have reached ~70.000 ha and have burned in Portugal); (ii) the intercept for the model proposed by Chaparro et al. (2016a), which reaches similar –even higher- values (depending on the interaction of the variables in that model); and (iii) the fact that under the present climate change conditions, a new type of wildfires, called "megafires", are increasingly frequent (e.g., recently >200.000 ha have burned in a single fire in Canada in 2019, and a similar situation happened in 2018 when four fires >100.000 ha burned in the country).

The map of potential burned area (Figure 24) is an example of the first application for fire risk assessment based on SMOS data for Europe. Now, thanks to the availability of SMOS-derived 1 km soil moisture maps over Europe (BEC, 2018), this product can be put on operational applications. To this purpose, it has been shown in this work that using SM data for a day before fire prediction allows developing such application (Figure 10).

4.4. Future work

With the purpose of enhancing the present results, the influence of the wind has been studied. However the relationship between burned area and wind speed is scarce (see Section 2.5) probably due to the fact that the resolution from the wind model applied is too coarse. Instead, wind effects are more complex and involve local factors (e.g., orography) and the change of wind direction. Also, synoptic

situations are needed to link wind and meteorological conditions to wildfire regimes (Duane and Brotons (2018).

Finally, other approaches could be studied to improve the reliability of the present model. First, remotely-sensed LST data could be derived from the Spinning Enhanced Visible and Infrared Imager (SEVIRI) sensor on board of Meteosat Second Generation satellites, in order to reduce the dependency on meteorological stations and to the get LST data every 15 minutes. However, note that this approach presents the limitation of cloud-masking in the infrared band. Secondly, the application of soil moisture and temperature anomalies to estimate fire propagation should be studied (Chaparro et al., 2016b). Thirdly, the applicability of microwave-derived L-band vegetation optical depth (VOD) as an estimate of biomass (Brandt et al., 2018; Rodríguez-Fernández et al., 2018; Chaparro et al., 2019) should be used to infer fuel availability, and the application of VOD to study vegetation water content conditions (e.g., Rao et al., 2019), should also be addressed.

5. Conclusions

Pre-fire conditions in the European Union have been analysed for the period 2010–2018 using the SMOS L4 high resolution soil moisture product, the ERA-5 land surface temperature data, CORINE land cover, ecoregions and month of the fire outbreak. Low temperatures and wet soils limited wildfires spread, while dry soils and high temperatures were linked to large burned areas.

Several models have been tested with different approaches. Firstly, estimates on burned area based on SM and LST have been performed using these variables in different linear regressions. Also, an additive term (σLogArea) has been summed to the intercept to avoid underestimation of fire propagation. Secondly, moisture and surface temperature have been joined in a bilinear regression, where SM has explained 25% of maximum fire spread, and LST 24% of the variance. In this case, the largest wildfires, ≥1,000 ha (i.e. $Log_{10}(Area)$≥ 3), are triggered by a moisture level below 0.10 m^3 /m^3 and temperatures higher than 300K. Thirdly, this model has been extended including land cover, ecoregions, and the month when fires burn. As expected, the largest wildfires take place in the southern region of Europe. Transitional woodland-shrub and burnt areas have been found as the land cover presenting a higher risk of fire spread. It is during the summer months that mores wildfires occur and are also the largest ones.

The comparison among the different models, and their validation, report that the model described in Eq. 2.3 (i.e., burned area as a function of soil moisture plus σLogArea) provides the best result (R^2 = 0.73; maximum error = 215 ha). Adding the standard deviation of the logarithm of burned area avoids underestimation and does not lead to overestimation effects, if compared to previous studies and to recent wildfires burning ~100.000 ha. From this model, a new operational application will arise: the SMOS Barcelona Expert Center will take profit of the new European SM maps at 1 km resolution to provide fire propagation risk maps in the European Union, based on the present work. Future work could enhance this model approach (e.g., including satellite-derived LST, moisture and temperature anomalies, VOD data, or wind information and synoptic situations) leading to enhanced estimates.

In conclusion, the proposed approach is valid for estimating the risk of propagation of wildfires in the European Union and has permitted to demonstrate and apply the high potentiality of L-band soil moisture data in fire risk assessment.

Acknowledgments

References

Albergel, C., Dutra, E., Munier, S., Calvet, J., Munoz-Sabater, J., De Rosnay, P., & Balsamo, G. (2018). ERA-5 and ERA-Interim driven ISBA land surface model simulations: Which one performs better? *Hydrology and Earth System Sciences, 22*(6), 3515-3532.

Aubrecht, C., Elvidge, C. D., Baugh, K., Hahn, S., & Jorge, N. (2011). Identification of wildfire precursor conditions: Linking satellite based fire and soil moisture data.

Bartsch, A., Balzter, H., & George, C. (2009). The influence of regional surface soil moisture anomalies on forest fires in Siberia observed from satellites. *Environmental Research Letters, 4*(4), 45021.

BEC (Barcelona Expert Centre). (2018). Land Variables. Retrieved from: http://bec.icm.csic.es/land-datasets. (s.f.).

Bossard, M., Feranec, J., Otahel, J., & Steenmans, C. (2000). *CORINE land cover technical guide-Addendum 2000.*

Brandt, M., Wigneron, J., Chave, J., Tagesson, T., Penuelas, J., Ciais, P., . . . Fensholt, R. (2018). Satellite passive microwaves reveal recent climate-induced carbon losses in African drylands. *Nature Ecology and Evolution, 2*(5), 827-835.

Chaparro, D., Duveiller, G., Piles, M., Cescatti, A., Vall-llossera, M., Camps, A., Entekhabi, D. (*in press*). Sensitivity of L-band vegetation optical depth to carbon stocks in tropical forests: comparison to higher frequencies and optical indices. *Remote Sensing of Environment.*

Chaparro Danon, D. "Applications of L-band missions for environmental research". Tesi doctoral, UPC, Departament de Teoria del Senyal i Comunicacions, 2018

Chaparro, D., Piles, M., Vall-Llossera, M., & Camps, A. (2016). Surface moisture and temperature trends anticipate drought conditions linked to wildfire activity in the Iberian Peninsula. *European Journal of Remote Sensing, 49*, 955-971.

Chaparro, D., Vall-Llossera, M., Piles, M., Camps, A., Rudiger, C., & Riera-Tatche, R. (2016). Predicting the Extent of Wildfires Using Remotely Sensed Soil Moisture and Temperature Trends. *IEEE Journal of Selected Topics in Applied Earth Observations and Remote Sensing, 9*(6), 2818-2829.

Duane, A., & Brotons, L. (2018). Synoptic weather conditions and changing fire regimes in a Mediterranean environment. *Agricultural and Forest Meteorology, 253-254*, 190-202.

ECMWF. European Centre for Medium-Range Weather Forecasts. (2019). https://www.ecmwf.int/en/forecasts/datasets

Entekhabi, D., Njoku, E., O'Neill, P., Kellogg, K., Crow, W., Edelstein, W., . . . Van Zyl, J. (2010). The soil moisture active passive (SMAP) mission. *Proceedings of the IEEE, 98*(5), 704-716.

ERA5-LST. (s.f.). https://www.ecmwf.int/en/forecasts/datasets/reanalysis-datasets/era5

FAO, 2006. FireManagement-Global Assessment 2006. A Thematic Study Prepared in the Framework. (s.f.).

Forkel, M., Thonicke, K., Beer, C., Cramer, W., Bartalev, S., & Schmullius, C. (2012). Extreme fire events are related to previous-year surface moisture conditions in permafrost-underlain larch forests of Siberia. *Environmental Research Letters, 7*(4).

Jolly, W., Cochrane, M., Freeborn, P., Holden, Z., Brown, T., Williamson, G., & Bowman, D. (2015). Climate-induced variations in global wildfire danger from 1979 to 2013. *Nature Communications, 6.*

Kerr, Y., Waldteufel, P., Wigneron, J.-P., Delwart, S., Cabot, F., Boutin, J., . . . Gruhier, C. (2010). The SMOS mission: new tool for monitoring key elements of the global water cycle The SMOS Mission: New Tool 2 for Monitoring Key Elements of. (5), 666-687.

LAND COVER. (s.f.). https://land.copernicus.eu/

Le Vine, D., Lagerloef, G., & Torrusio, S. (2010). Aquarius and remote sensing of sea surface salinity from space. *Proceedings of the IEEE, 98*(5), 688-703.

McArthur, A., & Australia. Forestry and Timber Bureau. (1967). *Fire behaviour in eucalypt forests.*

Metzger, M., Bunce, R., Jongman, R., Mücher, C., & Watkins, J. (2005). A climatic stratification of the environment of Europe. *Global Ecology and Biogeography, 14*(6), 549-563.

Metzger, M., Shkaruba, A., Jongman, R., & Bunce, R. (2012). EBONE EUROPEAN BIODIVERSITY OBSERVATION NETWORK.

Oppenheimer, M., Campos, M., Warren, R., Birkmann, J., Luber, G., O'Neill, B., ... & Hsiang, S. (2015). Emergent risks and key vulnerabilities.

Piles, M., Sánchez, N., Vall-Llossera, M., Camps, A., Martínez-Fernandez, J., Martinez, J., & Gonzalez-Gambau, V. (2014). A downscaling approach for SMOS land observations: Evaluation of high-resolution soil moisture maps over the Iberian peninsula. *IEEE Journal of Selected Topics in Applied Earth Observations and Remote Sensing, 7*(9), 3845-3857.

Portal, G., Vall-Llossera, M., Piles, M., Camps, A., Chaparro, D., Pablos, M., & Rossato, L. (2018). A spatially consistent downscaling approach for SMOS using an adaptive moving window. *IEEE Journal of Selected Topics in Applied Earth Observations and Remote Sensing, 11*(6), 1883-1894.

Rao, K., Anderegg, W., Sala, A., Martínez-Vilalta, J., & Konings, A. (2019). Satellite-based vegetation optical depth as an indicator of drought-driven tree mortality. *Remote Sensing of Environment, 227*, 125-136.

Rodríguez-Fernández, N. J., Mialon, A., Mermoz, S., Bouvet, A., Richaume, P., Al Bitar, A., ... & Kerr, Y. H. (2018). An evaluation of SMOS L-band vegetation optical depth (L-VOD) data sets: High sensitivity of L-VOD to above-ground biomass in Africa. *Biogeosciences, 15*(14), 4627-4645.

San-Miguel-Ayanz, J., Schulte, E., Schmuck, G., Camia, A., Strobl, P., Liberta, G., . . . Amatulli, G. (2012). Comprehensive Monitoring of Wildfires in Europe: The European Forest Fire Information System (EFFIS). En J. San-Miguel-Ayanz, E. Schulte, G. Schmuck, A. Camia, P. Strobl, G. Liberta, . . . G. Amatulli, *Approaches to Managing Disaster - Assessing Hazards, Emergencies and Disaster Impacts.* InTech.

Schmugge, T., O'Neill, P. E., & Wang, J. (1986). Passive microwave soil moisture research. IEEE Transactions on Geoscience and Remote Sensing, (1), 12-22.

UERRA. (2019). https://cds.climate.copernicus.eu/cdsapp#!/dataset/reanalysis-uerra-europe-height-levels?tab=overview

Ulaby, F. T., Moore, R. K., & Fung, A. (1981). *Microwave remote sensing: Active and passive. volume 1-microwave remote sensing fundamentals and radiometry.*

Van Wagner, C. (1987). *STRUCTURE OF THE CANADIAN FOREST FIRE WEATHER INDEX.*

Appendix: Supplementary tables

Table A1. Sample of the model described by Eq. (2.5)

	Variables	Number of fires	Percentage (%)
	Soil moisture	639	100,00
	Land surface temperature	639	100,00
Land cover	Agricultural areas	69	10,80
	Broad-leaved forest	23	3,60
	Coniferous forest	36	5,63
	Mixed forest	6	0,94
	Natural grasslands	41	6,42
	Moors and heathland	188	29,42
	Sclerophyllous vegetation	36	5,63
	Transitional woodland-shrub	108	16,90
	Sparsely vegetated areas	27	4,23
	Burnt areas	45	7,04
	Inland marshes	17	2,66
	Peat bogs	43	6,73
Months	January	6	0,94
	February	27	4,23
	March	77	12,05
	April	40	6,26
	May	34	5,32
	June	38	5,95
	July	116	18,15
	August	154	24,10
	September	65	10,17
	October	64	10,02
	November	10	1,56
	December	8	1,25
Ecoregions	North	38	5,95
	Central	81	12,68
	South	520	81,38